Revision 1

Monazite as a promising long-term radwaste matrix : benefits from high structural flexibility and chemical durability

N. Dacheux *, N. Clavier, R. Podor

ICSM – UMR 5257 CEA/CNRS/UM2/ENSCM, Site de Marcoule – Bât 426, BP 17171, 30207 Bagnols / Cèze, France

** Contact author :* Pr. Nicolas DACHEUX

ICSM – UMR 5257 CEA/CNRS/UM2/ENSCM
Site de Marcoule – Bât. 426
BP 17171
30207 Bagnols / Cèze cedex
France

Email : nicolas.dacheux@univ-montp2.fr

Abstract

Monazite ($Ln^{III}PO_4$) and related solid solutions are a well known source of rare earth elements on earth. They may also accommodate large amounts of thorium and uranium without sustaining damage to the structure by self-irradiation. Such observations led to monazite-type structures being proposed as a potential host matrix for sequestering long-lived radionuclides produced during the nuclear fuel cycle and/or plutonium and americium from dismantled nuclear weapons. Monazite has two main advantages as a radwaste matrix. The first is a high flexible structure that permits accommodation of high concentrations of actinides. The incorporation of trivalent elements may be obtained by direct synthesis of $An^{III}PO_4$ (An^{III} = Pu – Es), while tetravalent cation incorporation requires coupled substitutions, either on the anionic site (leading to monazite-huttonite solid solutions) or on the cationic site (monazite-cheralite solid solution). The various methods developed for the preparation of such compounds are summarized here, as well as the operating conditions required for the production of sintered pellets, with a particular focus on plutonium-bearing compositions. The second highly favorable property of monazite is its very high chemical durability. Several experimental procedures developed to determine normalized leaching rates are reviewed, as well as results obtained from natural and synthetic monazite. Potential phases formed during dissolution were considered because they strongly influence/control the concentration of actinides in the media. A preliminary list for such phases of interest, as well as corresponding thermodynamic data, is proposed.

Keywords

Monazite; Actinides; Leaching; Synthesis; Phosphate; Radwaste matrix

Introduction

The French Bataille's law related to nuclear waste management required to study potential conditioning of long-lived radionuclides, especially minor actinides and plutonium derived from dismantled nuclear weapons. To meet this law several dedicated ceramic materials were selected and extensively studied within the framework of NOMADE and MATINEX, which are large collaborative French Research Groups (CNRS/CEA/AREVA/EDF/French universities) (Dacheux et al. 2004; Terra et al. 2006). Three phosphate-based materials were identified as promising candidates on the basis of several properties that included ability to accommodate high concentrations of actinides (Dacheux et al. 2004), favourable response to sintering (Dacheux et al. 2002; Clavier et al. 2004; Montel et al. 2006), resistance to aqueous alteration (Oelkers et al. 2002; Poitrasson et al. 2004; Cetiner et al. 2005; Clavier et al. 2006a, 2006b; Dacheux et al. 2006, 2010; du Fou de Kerdaniel et al. 2007; Veilly et al. 2008), and radiation damage (Ewing and Haaker 1980; Karioris et al. 1981; Meldrum et al. 1998; Burakov et al. 2004; Bregiroux et al. 2007). The approach taken when selecting the materials was based on two steps. The first one, called « *Scientific Feasibility* », involved identifying materials that incorporated inactive actinide surrogates in their crystalline structures during synthesis, preparation of few grams of homogeneous material for complete materials characterization, evaluation of their response to sintering, then finally, their behaviour during leaching tests. This was followed by evaluating their "*Technical Feasibility*", which focussed on the preparation and characterization of actinide-based materials, the study of their structural stability under irradiation (samples doped with highly radioactive radionuclides (Deschanels 2006, Picot 2008), external irradiation, and study of natural analogues), and monitoring their long-term behaviour to enable the development of predictive models of their behaviour over time. Both steps argued for researchers to consider these properties in four matrices: britholites $Ca_9An^{III}_{1-x}An^{IV}_x(PO_4)_{5-}$

$_x(SiO_4)_{1+x}F_2$; monazite/cheralite solid solutions $Ln_{1-x-2y}An^{III}_xCa_yAn^{IV}_yPO_4$; Thorium Phosphate Diphosphate (β-TPD) with associated β-$Th_{4-x}An^{IV}_x(PO_4)_4P_2O_7$ solid solutions and combinations of monazite $Ln_{1-y}An^{III}_yPO_4$ / β-$TAn^{IV}PD$, and zirconolite $(Ca_{1-x}An_x)(Zr_{1-y}An^{IV}_y)Ti_{2-x}Al_xO_7$. (Dacheux et al. 2004, Guy et al. 2002).

There are several important reasons for considering monazite as a potential radwaste matrix, which include several geochemical considerations. From a geochemical point of view, monazite ($LnPO_4$ with Ln: La–Tb) is the most abundant lanthanide phosphate observed in natural samples (Förster 1998, Cuney and Mathieu 2000). It usually appears as an accessory mineral in granites, gneisses and pegmatites (Boatner 2002). It is also found in alluvial deposits and beach sands resulting from the weathering of the previously described host rocks. In addition to the major lanthanide element contents, many monazite samples contain large amounts of the natural radioactive elements thorium and uranium (Slodowska-Curie 1898; Overstreet 1967; Cuney and Mathieu 2000). As the major thorium source on earth, thorium contents in monazite ores can reach up to about 29 wt.% and 16 wt.% in ThO_2 and UO_2, respectively (Gramaccioli and Segalstad 1978; Boatner 2002; Lumpkin 1998). Individual samples of monazite may incorporate up to 50 wt.% of ThO_2 (Förster 1998; Förster and Harlov 1999; Montel et al. 2000). These results show that the monazite structure can accept large amounts of heavy actinide elements. Analyses of some natural samples have demonstrated a predominant coupled substitution between lanthanide elements and calcium + thorium (Kucha 1980; Rose 1980; Van Emden et al. 1997). The existence of a complete and ideal monazite-cheralite solid solution $M^{III}_{1-2x}M^{II}_xM^{IV}_xPO_4$ has been proven (Rose 1980).

Monazite's exceptionally high chemical stability also strongly argues for their use as a radwaste matrix (Lumpkin and Geisler-Wierwille 2012, Boatner 1988). Only few media, such as $CaCl_2$ or Pb-bearing fluids at 1000°C or alkali elements enriched fluids, induced significant dissolution/reprecipitation process with formation of secondary phases then discordancy

(Seydoux-Guillaume et al. 2002, Hetherington et al. 2008, Lumpkin G.R. and Geisler-Wierwille 2012). There are many documented cases where the mineral has survived multiple sedimentation and metamorphic cycles occurring over several hundred million years (Boatner 2002). Specific examples include the occurrence of ~2 Ga inherited monazite cores in younger metamorphic and igneous rocks (Rasmussen et al. 2007, Rasmussen et al. 2010, Paquette et al. 2004, Krenn et al. 2008) and, a comparative study between detrital monazite and monazite in the source rock from samples collected around Trolongnaro (Fort-Dauphin, Madagascar) (Montel et al. 2011) demonstrated that weathering, erosion and transport processes only mechanically abraded monazite, but did not chemically alter the mineral. Finally, detrital monazite grains constitute closed systems for the U-Th-Pb decay chains and allow geochronology demonstrates the capability of their structure to retain divalent elements (Montel et al. 2011). An additional indication of the high chemical durability of monazites comes from the extreme chemical conditions required to quantitatively dissolve natural monazite (concentrated H_2SO_4 at 210°C or concentrated NaOH at 140°C) for industrial applications (El-Nadi et al. 2005).

The resistance of the monazite structure to radiation damage is the third important parameter to consider in the field of long-term waste conditioning. Many minerals with large amounts of uranium or thorium are known to become more metamict over time. They thus became amorphous due to self-irradiation. The consequences of metamictization on the chemical (and mechanical) durability are more often explained by decrease of energy of cohesion associated to the damage of sample cristallinity (Roy and Vance 1981; Tamain et al. 2006, 2007). However, several authors have reported that natural monazite has never been found in the metamict state, which is probably due to the structures ability to self-anneal and recover easily its crystallization state (Boatner and Sales 1988, Lumpkin and Geisler-Wierwille 2012). Moreover, synthetic monazite samples exhibited a high resistance to

radiation damage (Ewing and Haaker 1980; Karioris et al. 1981; Meldrum et al. 1998; Burakov et al. 2004). Even though the critical amorphization temperature (i.e. temperature beyond which amorphization does not occur and only atomic scale defects are produced) ranged from 200°C to 300°C, monazite exhibits the same tendency for low temperature recovery and recrystallization as apatite and thus appears to be "radiation-resistant" (Ewing and Wang 2002). The negative consequence of amorphization are low since normalized dissolution rates for monazite are less than 2.6×10^{-3} $g.m^{-2}.d^{-1}$ (compared to $R_L < 10^{-3}$ $g.m^{-2}.d^{-1}$ for irradiated samples) even after heavy particle bombardment (Sales et al. 1983). Along similar lines, the preferential release of ^{238}U and ^{232}Th daughter products (i.e. ^{234}U, ^{230}Th, ^{228}Th) remained very low (increase by a factor of 1.1 to 10 relative to the structurally incorporated ^{238}U and ^{232}Th radionuclides) (Eyal and Kaufman 1982, Eyal and Olander 1990, Olander and Eyal 1990a,b). This isotopic fractionation was attributed to radiation damage in the tracks of the recoil nuclei emitted during α decay of the parent radionuclides and appeared to be dependent on the degree of radiation damage and the nature of the daughter products (Eyal and Olander 1990).

These geochemical and chemical considerations, and their consequences, argue for the use of monazite as a long-term radwaste host matrix, especially for actinides (Boatner and Sales 1988, Montel et al. 2011, Krauskopf 1986, Vance 2012). In this paper, we will only describe the impressive chemical flexibility of the monazite structure and the high chemical durability of synthetic materials doped with actinides that it imparts, even though the resistance of the ceramics to radiation damage can not be neglected.

1. Incorporation of actinides in the monazite structure : benefits from a great structural flexibility.

149 The AXO_4 monazite-type structure (monoclinic, space group $P2_1/n$, Figure 1) will
150 incorporate a remarkably wide range of elements, which makes it a ceramic material of
151 interest in several fields of research (Clavier et al. 2011). This surprising structural flexibility
152 is generally correlated to the low symmetry of the LnO_9 coordination polyhedron, which does
153 not induce severe charge or size constraints on which cations may be accommodated in the
154 site (Boatner et al. 1980b). Among the cations observed in the monazite structure, actinides
155 were generally observed in phosphate or silicate compounds. On this basis, several
156 substitution mechanisms were described and were found to be derived from two naturally
157 occuring accessory minerals *i.e.* monazite ($LnPO_4$) and associated cheralite
158 $Ln^{III}_{1-2x}M^{II}_{x}An^{IV}_{x}(PO_4)$, and huttonite ($ThSiO_4$).

159

160 The incorporation of trivalent actinides in the $LnPO_4$ monazite structure was readily
161 performed through the direct substitution of rare earth elements by actinides. Indeed, several
162 $An^{III}PO_4$ samples (An = Pu, Am, Cm, Bk, Cf and Es) are known to be stable (Bjorklund 1958;
163 Keller and Walter 1965; Haire et al. 1983; Hobart et al. 1983; Bregiroux et al. 2007b). This
164 was particularly interesting in the case of $EsPO_4$, which is one of the few einsteinium-based
165 compounds that has been synthesized at the weighable scale. Moreover, their preparation may
166 be completed via either wet or dry chemistry processes. On the one hand, wet chemistry
167 routes generally involved the initial precipitation of $An^{III}PO_4$. ½ H_2O rhabdophane
168 (hexagonal, space group $P6_222$) followed by heating of this intermediate phase between
169 800°C and 1500°C producing monazite-structure ceramics (Bjorklund 1958; Keller and
170 Walter 1965; Haire et al. 1983; Hobart et al. 1983). Through this approach, plutonium
171 monazite $PuPO_4$ was prepared by initially precipitating $Pu^{III}PO_4$. ½ H_2O rhabdophane from a
172 mixture of plutonium trichloride and $(NH_4)_2HPO_4$ between 75°C and 90°C, then firing the
173 precipitate above 950°C (Bjorklund 1958). The precipitation of $U^{III}PO_4$ in formic acid media

174 was also reported (Drozdziynski 1979) but this has been questioned given the high instability
175 of U(III) compared to U(IV) and U(VI) in phosphate-based media (Brandel 2004a,b). It is
176 also noted that wet chemistry routes can be used to control the final morphology of the
177 precipitate. For example, the addition of urea to an aqueous mixture of lanthanides and
178 ammonium phosphate was investigated and found to produce monodisperse powders with
179 grain sizes that varied as a function of the amount of urea added (Abraham et al. 1980;
180 Boatner 2002). On the other hand, solid state approaches to synthesis begin with a mixture of
181 powdered reagents followed by several cycles of grinding and heating. The repetition of such
182 cycles was generally required to reach the quantitative reaction between the powdered
183 precursors and avoid the presence of residual undesired secondary phases. As an example, the
184 preparation of $AmPO_4$ was successfully performed from a mixture of AmO_2 and $NH_4H_2PO_4$
185 fired two times at 1400°C (Bregiroux et al. 2007b). The direct substitution of trivalent
186 actinides on the cation site also led to the possible formation of complete solid solutions (such
187 as $La_{1-x}Pu_xPO_4$ (Burakov et al. 2004; Popa et al. 2007) and $La_{1-x}Am_xPO_4$ between pure end-
188 members (Abraham et al. 1980; Anderson and Burakov 2004; Kitsay et al. 2004; Zhang and
189 Vance 2008)). Single crystals of $LaPO_4$ doped with ^{241}Am or ^{246}Cm were also grown from a
190 $Pb_2P_2O_7$ flux then separated from solidified flux by mechanical steps and/or boiling in
191 concentrated HNO_3 (Kelly et al. 1980, Boatner et al. 1980b).
192
193 In contrast to the incorporation of trivalent actinides in the monazite structure,
194 accommodation of actinides with higher oxidation states generally required coupled
195 substitutions, either on the cationic or on the anionic site. However, a direct mechanism of
196 incorporation, based on the replacement of 4 REE^{III} by 3 An^{IV} and the simultaneous formation
197 of a vacancy, was also reported in natural and synthetic samples (Podor 1994) :
198

199 $$4\ Ln^{III} \leftrightarrow 3\ (Th,U)^{IV} + \square \qquad (1.)$$

200

201 However, this substitution appeared to limit the incorporation of thorium and uranium
202 to a few wt% in natural monazites and up to 18 wt% ThO_2 in synthetic samples (Podor 1994).
203 Other authors have also argued for the direct incorporation of up to 10 wt% UO_2, PuO_2 or
204 NpO_2 in $LaPO_4$ (Boatner et al. 1980a; Kelly et al. 1981). A second mechanism involving the
205 formation of vacancies in the structure required the simultaneous incorporation of divalent
206 elements :

207

208 $$(1-x)\ Ln^{III}PO_4 + x/6\ M^{II} + 2x/3 An^{IV} + x\ PO_4^{3-} + x/6\ \square \leftrightarrow Ln^{III}_{1-x} M^{II}_{x/6} An^{IV}_{2x/3} \square_{x/6} (PO_4) \qquad (2.)$$

209

210 This mechanism led to the $M^{II}_{0.5} An^{IV}_2 (PO_4)_3$ family which was studied by Orlova *et al.*
211 with An^{IV} = Np, Pu (Kitaev et al. 2004). Nevertheless, these compounds were prepared
212 through crystal growth methods involving Pb/PbO melts that might induce the presence of
213 significant amounts of lead in the final samples, leading to a cheralite-type substitution (see
214 below). These compounds were never considered for the immobilization of actinides because
215 of the probable decrease in chemical durability caused by the presence of vacancies in the
216 structure (Horlait et al. 2012a, Horlait et al. 2012b).

217 Two approaches were taken to avoid the formation of such crystal defects during the
218 incorporation of tetravalent actinides in the monazite structure. The first one involved the
219 substitution of Ln^{III} by An^{IV} coupled with the substitution of phosphate by silicate groups
220 such as :

221

222 $$(1-x)\ Ln^{III}PO_4 + x\ An^{IV} + x\ SiO_4^{4-} \leftrightarrow Ln^{III}_{1-x} An^{IV}_x (PO_4)_{1-x} (SiO_4)_x \qquad (3.)$$

223

Only a few complete studies reported a full and complete characterization of the substitution in such systems (Hikichi et al. 1978) and are mainly based on natural analogues containing high thorium contents (Montel et al. 2011). Indeed, monoclinic $ThSiO_4$ (huttonite) (Hutton 1951), as well as $PaSiO_4$ (Keller 1963; Myasoedov et al. 2006), are stable actinide silicates with the monazite structure, even if thorium silicate is most commonly known in its tetragonal form, called thorite. Tetravalent uranium, neptunium, plutonium and americium silicates also crystallize in such zircon-type structure (Keller 1963; Speer 1980; Pointeau et al. 2009). Some recent work on detrital monazite with both uranium and thorium from Trolognaro (Madagascar) revealed that uranium was preferentially associated to calcium in a monazite-cheralite type solid solutions (through $M^{III} \Leftrightarrow (M^{II}+M^{IV})$ substitution) while thorium involved a coupled mixed substitution $(M^{III} + PO_4) \Leftrightarrow (M^{IV} + SiO_4)$, leading to the formation of a monazite-huttonite solid solution (Montel et al. 2011). Furthermore, it is noted that this latter mineral family also exhibits long-term durability in geological media (Helean et al. 1999) and was proposed as a host matrix for the immobilization of weapon-grade plutonium (Ewing 2007; Ewing et al. 1995) and the treatment of highly radioactive liquid ^{241}Am waste generated by the metal to oxide conversion of plutonium derived from dismantled nuclear weapons (Aloy et al. 2001).

The second mechanism reported in the literature, and by far the most well-documented, for the incorporation of tetravalent actinides in the monazite structure leading to the formation of $Ln^{III}_{1-2x}An^{IV}_{x}M^{II}_{x}(PO_4)$ compounds is generally called “cheralitic substitution” (with reference to cheralite, previously reported as brabantite (Linthout 2007)) :

$$(1 - 2x)\ Ln^{III}PO_4 + x\ An^{IV} + x\ M^{II} + 2x\ PO_4^{3-} \leftrightarrow Ln^{III}_{1-2x}M^{II}_{x}An^{IV}_{x}(PO_4) \qquad (4.)$$

Due to their common occurrence in natural samples, thorium and uranium were the most studied tetravalent actinides in cheralite. Indeed, the preparation of $Ca_{0.5}Th_{0.5}PO_4$, in inert or reducing atmosphere (Davis et al. 1981), and of $Ca_{0.5}U_{0.5}PO_4$, as well as associated solid solutions with $LnPO_4$, was reported possible by dry chemistry experiments (Bregiroux et al. 2007c). Such chemical routes were usually based on powdered mixtures of AnO_2 and $M^{II}O$ oxides and $NH_4H_2PO_4$, which were ground and fired several times to obtain homogeneous single phase monazite-type compounds at high temperature. Conversely, wet chemistry methods, including those involving hydrothermal conditions, have so far failed to prepare pure and single phase compositions on the cheralite-monazite solid solution (Podor et al. 1995; Podor and Cuney 1997). This is also the case for uranium-based equivalents, the synthesis experiments for which have produced polyphase products composed by $Ca_{0.5}U_{0.5}PO_4$ and $U_2(PO_4)(P_3O_{10})$ (Muto et al. 1959, Podor et al. 2003). Similarly, the formation of $HTh_2(PO_4)_3$ and ThP_2O_7 in the mixtures resulting from hydrothermal reactions was commonly observed in experiments designed to prepare pure $Ca_{0.5}Th_{0.5}PO_4$ (Podor 1994); these also contributed to the production of polyphase samples composed by cheralite and thorium-phosphate diphosphate (du Fou de Kerdaniel 2007).

Neptunium and plutonium have also been stabilized in monazite in the tetravalent oxidation state. Pure end-member $Ca_{0.5}Np^{IV}_{0.5}(PO_4)_2$ was synthesized via a dry chemistry route (Raison et al. 2008). However, the replacement of calcium by another divalent cation was found to induce a slight structural change, leading to a substance of cheralitic-composition with an orthorhombic structure (space group *Cmca*) for $Sr_{0.5}Np_{0.5}PO_4$ (Popa et al. 2010). On the other hand, plutonium was a special case since it was stabilized with both III and IV oxidation states. Although the stabilization of trivalent plutonium $Pu^{III}PO_4$ was readily achievable via different chemical synthesis mechanisms, attempts to incorporate pure

tetravalent plutonium in the monazite structure, producing $M^{II}_{0.5}Pu^{IV}_{0.5}(PO_4)$ cheralite, always failed and produced samples exhibiting mixed oxidation states. Indeed, even if the steric criterion reported by Podor and Cuney (1997) are satisfied for such compounds, Pu^{IV} was easily reduced to the trivalent oxidation state during the experiment thus limiting the availability of Pu^{IV} for incorporation in the monazite structure. Indeed, under argon or inert atmospheric conditions, plutonium was fully reduced to Pu^{III}, which is the most stable oxidation state of plutonium in phosphate media, and only $PuPO_4$ was obtained (Bregiroux et al. 2007b). Even when preparing the material in air and using Ca^{2+} as a charge compensator, resulted in the formation of $Pu^{III}_{0.4}Ca^{II}_{0.3}Pu^{IV}_{0.3}(PO_4)$ (Bregiroux et al. 2007b). Very similar results were obtained when trying to incorporate the analogous tetravalent cerium in the monazite structure (Pepin et al. 1981; Bregiroux et al. 2007c). However, the presence of another tetravalent actinide in the system seems to partly stabilize Pu^{IV}, as in the example of $Ca^{II}_{0.5}Np^{IV}_{0.35}Pu^{IV}_{0.15}(PO_4)$ that was prepared by Tabuteau *et al.* (1988). Pentavalent neptunium and plutonium were never observed in the monazite structure (Vance et al. 2011).

All the M^{II}/An^{IV} couples reported in the literature are summarized in Table 1. Many intermediate compounds between the pure cheralite end-members have also been successfully prepared, particularly the thorium and uranium form (Clavier *et al.* 2011). The diversity and range of compositions that can be synthesized, which can be extended to all the $An^{III}PO_4$ compounds, demonstrates that the monazite structure appears to be particularly suitable for the immobilization of actinides. Indeed, from a preparation and synthesis perspective, monazite fulfills several crucial criterion required for radwaste matrices *i.e.* high weight loading in actinides, capability to host tri- and tetravalent radionuclides simultaneously, and adaptability of the routes used to chemically prepare the material (from powder metallurgy to dustless wet chemistry methods) (Table 2). Also, it is noted that other stable compounds with the monazite structure (such as $Na_3(Pu,Am)_2(PO_4)_3$ and $K_3(Am,Cm)_2(PO_4)_3$) are reported in

the literature but were not envisaged as radioactive waste matrices (Burnaeva et al. 1992; Volkov et al. 2002), probably because the presence of the monovalent cation could drastically decrease the chemical durability of such samples. Similarly, thorium-containing vanadates (Calestani et al. 1984, Nabar and Mahtre 1987, 2001) and arseniates (Nabar and Sakhardande 1985, 1999), as well as pure $PuAsO_4$ and $AmAsO_4$ end members (Keller and Walter 1965) were prepared; they too belong to the actinide-bearing monazite group.

The second property required of an actinide-bearing conditioning material is its response to sintering. High density pellets of actinide-containing compounds with a monazite-type structure were prepared by high temperature sintering of powders to demonstrate the feasibility of monazite manufacturing and/or to perform chemical durability tests. The optimum sintering temperature reported for $LnPO_4$ monazites (doped or not with actinides) generally ranges from 1350 to 1500°C (Bregiroux et al. 2006, 2007a; Cho et al. 2009, Aloy et al. 2001), although this may be slightly lowered when sintering nanopowders (Rajesh et al. 2004). Without any additives and/or additional external pressure, densification rates up to 98% of the calculated value were obtained. Also, grain growth may be controlled to tailor the final average grain size in the samples: slow heating rates are needed to reach higher density values and avoid the inhibition of grain growth by porosity (Bregiroux et al. 2009). The sintering of lanthanide phosphates also appears to be limited by phosphate decomposition and/or by the presence of impurities (Morgan et al. 2005). In particular, the presence of residual polytrioxophosphate species in the samples, $Ln(PO_3)_3$, was found to induce the formation of a glassy phase surrounding the grains (Hernandez and Martin 2008) as well as promote abnormal grain growth which led to the formation of numerous intragranular pores (Bregiroux et al. 2006).

Very few papers report the response to sintering of monazite-cheralite solid solutions containing actinides (Terra et al. 2006). Nevertheless, all published results agree that their response to sintering is similar to $LnPO_4$. For example, a 95% densification rate for Th-bearing samples was achieved after 4 hours of heating at 1450°C (Montel et al. 2006; Glorieux et al. 2009). Similar relative densities were reported when performing densification through a reactive sintering process : in this case, a mixture of $CaHPO_4.2H_2O$, ThO_2 and $NH_4H_2PO_4$ was mechanically ground, pre-treated at 800-900°C, ground again, shaped then fired at 1300°C to simultaneously form the cheralite phase and to obtain dense pellets (figure 2) (Terra et al. 2006).

2. Evidence for remarkable chemical durability

2.1. Dissolution tests

The stability of natural monazites in alluvial deposits or beach sands, as well as the extreme conditions required to dissolve and quantitatively recover thorium or uranium from monazites, argue for a remarkable chemical stability. To test that synthetic samples (monazite, monazite-cheralite, cheralite) conform to observations made on natural samples, normalized dissolution rates were evaluated using several leaching tests developed using either static (low renewal of the leachate, e.g. 10^{-1} $mL.d^{-1}$) or dynamic (high renewal, e.g. 0.5 and 50 $mL.h^{-1}$) conditions (Figure 3). High density polyethylene (HDPE) or polytetrafluoroethylene (PTFE) vessels were usually used to avoid adsorption of released elements on the containers walls (Ranney and Parker 1998). Prior to dissolution tests, sintered pellets or powdered samples were first washed for several days in 10^{-1}M HNO_3 at room temperature to remove minor phases or crystal defects at the surface of the samples that may

348 generate a bias in the element release from the surface of the samples in the early stages of the
349 experiments. For static experiments, the slow leaching flow rate did not significantly impact
350 the system and usually enabled examination of the behaviour of the pellets close to the point
351 of solubility equilibrium, *i.e.* when saturation conditions are reached in the leachate.

352 Conversely, dynamic-type leaching tests avoid the thermodynamic consequences of
353 neoformed phases at the surface of the leached samples, and by extension, avoid the
354 discrepancies that such phases may introduce when determining leaching rates. Rapid
355 removal of the leachate was achieved by the means of PTFE leaching flow reactor (Dacheux
356 et al. 2010) in which powdered samples were placed in contact with acidic solution. The
357 circulation of the leaching solution was achieved by a peristaltic pump that ensured complete
358 renewal of the leachate fluid twice an hour. The temperature of the experimental set-up was
359 adjusted by the means of an aluminium dry-bath, and varied between room temperature and
360 90°C. Higher temperatures were achieved in a similar experimental set-up by use of titanium
361 autoclaves (Deberdt et al. 1998). Regular aliquots extracted from the experiments were
362 centrifuged to remove colloids then elemental concentrations were determined by
363 conventional techniques, including Inductively Coupled – Atomic Emission Spectroscopy
364 (ICP-AES) or Mass Spectrometry (ICP-MS) and PhotoElectron Rejecting Alpha Liquid
365 Scintillation (PERALS).

366

367 *2.3. Determination of the normalized dissolution rates*

368 To make accurate comparisons between the various materials studied, and the different
369 experimental techniques, the results for element leachability, *i,* were normalized to determine
370 a value of $N_L(i)$ (expressed in $g.m^{-2}$), i.e. considering Eq.5 and Eq.6. for static (Dacheux et al.
371 2006) and dynamic (Wintergerst et al. 2009) leaching experiments, respectively.

$$N_L(i) = \frac{m_i}{f_i \times S} \quad (5.)$$

$$N_L(i, t + \Delta t) = \frac{C_i(t) \times d \times \Delta t}{f_i \times S} + N_L(i, t) \quad (6.)$$

For static experiments, m_i is the total amount of *i* measured in solution (g), *S* the effective surface area (m^2) of the pellet in contact with the solution and f_i is the mass ratio of the element *i* in the solid. For dynamic experiments, $N_L(i, t + \Delta t)$ and $N_L(i, t)$ correspond to the cumulative normalized leachings for *i* element for a leaching time equal to t and $t + \Delta t$, respectively; t and $t + \Delta t$, the cumulative leaching times (hours or days), respectively, and Δt, the time interval between two withdrawals ; $C_i(t)$, the concentration of the element *i* and *d*, the water flow rate ($L.d^{-1}$)**.**

The normalized dissolution rate R_L ($g.m^{-2}.d^{-1}$), which stands as the mass loss of the dissolved material per unit time and surface units, was determined from the evolution of the normalized leachings, N_L ($g.m^{-2}$), and calculated using the equation presented by Dacheux et al. (2006) :

$$R_L(i) = \frac{dN_L(i)}{dt} \quad (7.)$$

By this approach, the chemical durability of the samples is normalized to the reactive surface of the solid in contact with the solution and by the elementary weight loading. When the dissolution occurred far from equilibrium, the normalized dissolution rates were usually found to be constant (Dacheux et al. 2006) and are noted $R_{L,0}$. Conversely, near the establishment of equilibrium, saturation processes associated with the precipitation of neoformed phases onto the surface of the solids occurs, and generally led to a decrease of normalized dissolution rates. The associated value, which corresponds to the release of the

393 elements from the crystalline matrix followed by a diffusion step through the surface layer
394 was then distinguishable from the real normalized dissolution rate and is noted $R_{L,t}$ (Dacheux
395 et al. 2006) (Figure 3).
396
397 *2.3. Dissolution of $LnPO_4$ monazites*
398
399 Despite their wide abundance in the geosphere coupled to an increasing economic
400 interest (Alonso et al. 2012), the dissolution of lanthanide bearing monazites appears to be
401 poorly documented in the literature. Indeed, only a few studies deal with the behaviour of
402 natural samples, and even fewer are dedicated to synthetic materials (Aloy et al. 2001, Terra
403 et al. 2003; Kamel et al. 2010).
404 From a geochemical perspective, the alteration of monazite was frequently
405 investigated at non-ambient hydrothermal conditions since its interaction with aqueous fluids
406 is one of the major factors controlling rare earth element and thorium mobility in crustal
407 fluids (Schmidt et al. 2007). In this context, extreme experimental conditions, typically about
408 T = 700-1000°C and P = 1-2 GPa, are frequently used (Pourtier et al. 2010; Tropper et al.
409 2011). Nevertheless, monazite still appears to be highly durable, with the time needed to
410 completely dissolve 5 μm or 10 μm crystals calculated to be $t < 50{,}000$ years or $t < 100{,}000$
411 years, respectively; as although these are still deemed to be "rapid" at the geological timescale
412 (Rapp and Watson 1986). Also, no fractionation between light (LREE : La - Sm) and heavy
413 rare earth elements (HREE : Gd - Lu) was observed, meaning that the dissolution remained
414 congruent over the whole composition range (Poitrasson et al. 2000). Conversely, the long-
415 term degradation of monazite from Steenkampskraal mine (South Africa) was studied through
416 an integrated geological, hydrogeological and mineralogical approach and revealed the

417 preferential release of heavy rare-earths and enrichment in thorium after leaching (Read
418 2002).

419 Even if the studies dedicated to the aqueous geochemistry of monazites stated their
420 very high chemical durability, they often lacked data of absolute dissolution rates. Indeed,
421 only general trends or solubility measurements were reported (Poitrasson et al. 2004; Cetiner
422 et al. 2005). The studies conducted in less aggressive environments allowed the determination
423 of normalized dissolution rates in various experimental conditions, as well as evaluation of
424 several parameters such as temperature, pH or nature of the complexing ligand. Whatever the
425 media and the nature of the sample considered (natural or synthetic), the chemical durability
426 of monazite always appeared to be very high. Indeed, the R_L(La) values determined during the
427 dissolution of natural monazite samples from Manangotry (Madagascar) at pH = 2 varied
428 between about 5×10^{-7} $g.m^{-2}.d^{-1}$ (T = 50°C) and 10^{-4} $g.m^{-2}.d^{-1}$ (T = 200°C) (Oelkers and
429 Poitrasson 2002) and an apparent activation energy of about 40 $kJ.mol^{-1}$. This is in good
430 agreement with the data reported for other phosphate-based ceramics (Thomas et al. 2001;
431 Robisson et al. 2002; Dacheux et al. 2006) and is characteristic of surface controlled
432 dissolution. The normalized dissolution rates were always found to vary as a function of the
433 leachate acidity and reached a minimum value for near-neutral pH with $R_L \approx 5 \times 10^{-8}$ $g.m^{-2}.d^{-1}$
434 . These results, obtained on natural samples, were comparable to data collected during the
435 dissolution of synthetic Gd-monazite sintered pellets at 90°C (Terra et al. 2003). With less
436 than one order of magnitude between both data sets (Table 3), synthetic samples exhibited
437 almost the same chemical durability as natural analogues, provided that homogeneous and
438 single phase samples were prepared (Terra et al. 2003). The high chemical durability of
439 monazite was also confirmed in the presence of organic media, such as in humic acid
440 solutions (Polyakov et al. 2009; Goyne et al. 2010).

441 The measured normalized dissolution rates of monazite are several orders of
442 magnitude lower than those reported for other ceramic materials studied, such as britholite
443 (Dacheux et al. 2010) or zirconolite (Leturcq et al. 2001), but similar to those for Thorium
444 Phosphate-Diphosphate (β-TPD) (Robisson et al. 2002; Dacheux et al. 2004, 2006) or β-
445 TPD/monazite composites (Clavier et al. 2006a). Monazite may thus be considered as durable
446 as β-TPD which is one of the least soluble inorganic phases reported in the literature (Sillen
447 and Martell 1964). Sales et al. (1983) also argued that La-monazite leaching rates are about
448 1000 times lower than borosilicate glasses. However, they based their conclusions on results
449 from MCC-1 type leaching tests (distilled water, T = 90°C, S/V = 0.1 cm^{-1}, *t* = 28 days) which
450 did not take into account the possible precipitation of neoformed phases in the back-end of the
451 initial dissolution process. Indeed, such method is based on a single data point determined
452 from the concentrations in the leachate after 28 days and therefore supposed that the evolution
453 of the elementary releases is linear. Conversely, the values reported by Kamel et al. (2010) are
454 significantly higher than those reported elsewhere in the literature (6 $g.m^{-2}.d^{-1}$ at pH = 1). This
455 lower chemical durability was assigned to the chemical routes used for monazite preparation
456 (sol-gel or dry methods) that induced the formation of less durable secondary phases.
457 The dissolution of La-monazite sintered samples doped with high ^{241}Am radioactivity
458 (specific activity of 2.13×10^{7} $Bq.g^{-1}$) was also examined in distilled water at 90°C. The
459 normalized dissolution rates ranged between 1.2×10^{-4} $g.m^{-2}.d^{-1}$ for $R_L(La)$ and 2.3×10^{-4}
460 $g.m^{-2}.d^{-1}$ for $R_L(Am)$, which are of the same order of magnitude to those of undoped ceramics
461 (Aloy et al. 2001). On this basis, the self-irradiation of the sample, as well as the alpha
462 radiolysis, do not appear to significantly influence the dissolution kinetics.
463
464 *2.4. Dissolution of actinide-bearing cheralite and monazite-cheralite solid solutions*
465

Literature dealing with the chemical durability of synthetic cheralite (and monazite-cheralite solid solutions) is almost inexistent. Only few results were recently published on the dissolution of homogeneous and single phase $CaTh^{IV}_{0.5-x}U^{IV}_{x}(PO_4)$ at 90°C in 10^{-1} and 10^{-4}M HNO_3 (Terra et al. 2003; du Fou de Kerdaniel et al. 2007; Veilly et al. 2008). What data there is reveals two different behaviors for the typical evolution of normalized leaching (Figure 4), which depend on the chemical composition considered.

The dissolution of sintered $Ca_{0.5}Th_{0.4}U_{0.1}PO_4$ was mainly characterized by the rapid precipitation of thorium while uranium was released into solution ($R_L(U) \approx 2.4 \times 10^{-4}$ $g.m^{-2}.d^{-1}$), probably due to its oxidation to a uranyl molecular ion at the surface of the leached material. When studying various monazite samples, Eyal and Olander (1990) also reported non-stoichiometric leaching of the actinide elements due to different transport properties (especially in presence of carbonate species). Moreover, the $R_{L,0}(U)$ value determined agreed well with those reported for natural samples of monazite-cheralite solid solutions (Sales et al. 1983; Oelkers and Poitrasson 2002). For longer leaching times, uranium release significantly slowed down ($R_{L,t}(U) \approx 2.5 \times 10^{-5}$ $g.m^{-2}.d^{-1}$) probably due to the formation of a passivative thorium-enriched layer at the surface of the leached pellet (like in Clavier et al. 2006b). This layer acted as a diffusion barrier for uranium, as suggested by the linear evolution of $N_L(U)$ versus the square root of time (Lasaga 1998) (Figure 4b). The behaviour of pure $Ca_{0.5}U_{0.5}PO_4$ end-member differed significantly from that of $Ca_{0.5}Th_{0.4}U_{0.1}PO_4$. Its solubility was mainly controlled by kinetics ($R_{L,0}(U) \approx 4.2 \times 10^{-6}$ $g.m^{-2}.d^{-1}$) and did not involve any saturation phenomena, probably because of the absence of thorium in the sample. However, the normalized dissolution rate of powdered $Ca_{0.5}U_{0.5}PO_4$ remained very low since no alteration was observed by XRD after 3 weeks of contact with deionized water at 200°C and 300 bars (Davis et al. 1981).

For comparison purposes, the dissolution of $La_{0.4}Eu_{0.1}Ca_{0.25}Th_{0.25}PO_4$ and $La_{0.4}Eu_{0.1}Ca_{0.25}U_{0.25}PO_4$ monazite-cheralite solid solutions was also examined in 10^{-1}M HNO_3 at 90°C (Table 4). As observed for pure cheralite, the nature of the actinides incorporated in the monazite-type structure significantly affected the behaviour of the material during leaching tests. Materials such as $La_{0.4}Eu_{0.1}Ca_{0.25}Th_{0.25}PO_4$ sample exhibited two orders of magnitude higher chemical durability (1.7×10^{-6} g.m^{-2}.d^{-1} < $R_{L,0}$(Ln) < 4.3×10^{-6} g.m^{-2}.d^{-1}) than $La_{0.4}Eu_{0.1}Ca_{0.25}U_{0.25}PO_4$ ($2 - 4 \times 10^{-4}$ g.m^{-2}.d^{-1}). Moreover, the rapid precipitation of thorium at the solid/liquid interface induced a decrease of the normalized dissolution rate by at least one order of magnitude ($R_{L,t}$(Ln) ≈ 10^{-7} g.m^{-2}.d^{-1}) after only 7 days of leaching. Conversely, uranium did not precipitate in the experiments. The dissolution of $La_{0.4}Eu_{0.1}Ca_{0.25}U_{0.25}PO_4$ was found to be congruent during the early stages of leaching since uranium, lanthanum and europium releases were similar.

The substitution of thorium by uranium (IV) in the structure led to an increase of the normalized dissolution rate by two orders of magnitude. The decrease of the chemical durability was probably linked to the oxidation of uranium (IV) to UO_2^{2+} at the interface between the solid and the solution, weakening the cohesion of the lattice (Veilly et al. 2008) then enhancing the release of uranium in solution. The formation of uranyl phosphate pentahydrate, $(UO_2)_3(PO_4)_2$. 5 H_2O (log K_S = -55.1 ± 0.9) and the less soluble thorium phosphate-hydrogenphosphate hydrate $Th_2(PO_4)_2(HPO_4) \cdot H_2O$ (log K_S = -66.6 ± 1.1) near the point of saturation explains the different behaviour of thorium and uranium (Thomas et al. 2001; du Fou de Kerdaniel et al. 2007; Robisson et al. 2002; Clavier et al. 2006b; Tamain et al. 2007). The rapid formation of lanthanide phosphate (either in the rhabdophane or hydrated monazite form) also occurred at the solid/liquid interface (du Fou de Kerdaniel et al. 2007; Clavier et al. 2006), leading to a significant decrease of the lanthanide concentration in the leachate and to the establishment of diffusion phenomena.

515 However, despite the presence of redox phenomena, the normalized dissolution rates
516 determined for uranium-bearing monazite-cheralite solid solution during the first days of
517 leaching remained very low compared to other ceramics studied. From this point of a view,
518 monazite, compared to britholite, combines an important structural flexibility with an
519 impressively high chemical durability. In the case of britholite, its favorable properties in
520 terms of actinide loading, which are related to a channel-framed structure, may be responsible
521 for the much lower durability during dissolution tests. The contrasting behavior was examined
522 in the light of periodic DFT calculations, especially when considering the promotor effect in
523 both matrices (Veilly et al. 2008). This promotor effect was significant in thorium bearing
524 britholites, but remained very low for thorium bearing monazite-cheralite solid solutions. In
525 such conditions, calcium atoms should be less easily released from monazite due to a higher
526 cohesive energy, suggesting that the high resistance of the monazite structure to aqueous
527 alteration may be due to the distorted and flexible cationic environment in such structure.
528
529 To account for the influence on normalized leaching rates caused by the rapid
530 precipitation of neoformed phases, the dissolution of several $Ca_{0.5}Th_{0.5-x}U_xPO_4$ solid solutions
531 were studied in dynamic conditions, *i.e.* with high and continuous renewal of the leaching
532 solution (Figure 5, Table 3). Comparison of the normalized dissolution rates determined in 10^{-1}
533 M HNO_3 at 70°C illustrates once again the key role of uranium on the chemical durability of
534 the cheralite matrix. Indeed, the R_L values obtained from uranium release into solution were
535 found to increase by about one order of magnitude when x varied between 0.1 and 0.3 before
536 reaching a plateau. The precipitation of thorium was not avoided even for such high leachate
537 renewal rates. Conversely, the dissolution of cheralite samples with lower uranium contents (x
538 $\leq$ 0.2) appeared to be controlled only by kinetics since the variation of the normalized
539 leaching rates versus time was found to be strictly linear, even after several days of contact

between the solid and the solution. At these conditions, the slope in the evolution of the normalized weight loss reflects the true dissolution rate of the solid, *i.e.* exempt from any perturbation due to surface precipitation.

Finally, it is generally agreed in the abundant literature from the fields of geochemistry and chemistry (Furrer and Stumm 1986; Ganor et al. 1995; Walther 1996; Pokrovsky and Schott 2000; Heisbourg et al. 2003, 2004), that the normalized dissolution rates determined for monazite-like samples were systematically found to increase with the proton concentration in 10^{-1}-10^{-4}M HNO_3. Nevertheless, the influence of acidity was found to be moderate since the R_L values were only doubled between pH = 4 and pH = 1. Whatever the chemical composition of the samples, such fractional and low dependence (partial order related to the proton activity of 0.1-0.2) (Table 5) has been discussed by several authors, and relates directly to the concentration of active sites at the solid/liquid interface, and by extension is a surface reaction controlled dissolution.

2.5. Thermodynamic aspects of the monazite-cheralite dissolution

Phosphate-based neoformed phases are usually rapidly developed at the solid/liquid interface shortly after the establishment of saturation processes when dissolving phosphate-based ceramics. It is well known that such phases are associated with very low solubility constants and thus to high retention of actinides (Table 6). For trivalent elements, the nature of the precipitated phases is controlled by several parameters (ionic radius of the trivalent element, temperature and time, supersaturation index). For example, at 150°C, monazite (monoclinic, $P2_1/n$) is formed for lanthanum and cerium, rhabdophane (hexagonal, $P6_222$) from neodymium to dysprosium and xenotime (tetragonal, $I4_1/amd$) for heavy lanthanides (Ho-Lu) (du Fou de Kerdaniel et al. 2007). When extending the study to other temperatures,

565 monazite is clearly stabilized at higher temperatures compared to rhabdophane (which
566 constitutes a low-temperature actinide-phosphate form). This is in good agreement with
567 geological observations in the literature where monazite is more common than the rarely
568 observed rhabdophane. On the basis of steric considerations, americium and curium should
569 thus be precipitated as $(Am,Cm)PO_4 . ½ H_2O$ rhabdophane up to 170°C, and as monazite-type
570 minerals at higher temperatures (du Fou de Kerdaniel et al. 2007). For trivalent plutonium, the
571 rhabdophane to monazite transition should occur between 140°C and 150°C. Such results
572 appear in good agreement with those reported by Keller and Walter (Keller and Walter 1965)
573 who precipitated crystalline Am-rhabdophane samples from a supersaturated mixture of
574 Na_2HPO_4 and Am(III) nitrate solution under hydrothermal conditions at 150°C. They also
575 reported the transformation of Am-rhabdophane to Am-monazite above 200°C. As previously
576 stated, $PuPO_4 . ½ H_2O$ also formed by precipitation and was found to be stable with very low
577 solubility in various acidic and basic concentrated media (Bjorklund 1957).

578 The behaviour of tetravalent elements in the presence of phosphate species is also
579 described in literature. In anoxic conditions, tetravalent thorium, plutonium and uranium are
580 usually precipitated as $An_2(PO_4)_2(HPO_4).H_2O$ (Dacheux et al. 2007b) previously identified as
581 $An_3(PO_4)_4.xH_2O$ or $HAn_2(PO_4)_3.yH_2O$ (Cleveland 1970, King 1949). On the other hand, in
582 oxidizing conditions, tetravalent uranium is oxidized to uranyl ions and forms $(UO_2)_3(PO_4)_2 .$
583 $5H_2O$ (du Fou de Kerdaniel et al. 2007, Thomas et al. 2001). While the dissolution of
584 monazites should all follow the same trend, the behavior of monazite-cheralite solid solutions
585 may vary due to the incorporation of divalent elements. The precipitation of tetravalent
586 elements with phosphate species in the presence of large amounts of calcium was examined
587 using super-saturation experiments. It was found that an original rhabdophane-type solid of
588 formula $Nd_{0.8}Ca_{0.1}Th_{0.1}PO_4 . ½ H_2O$ was rapidly precipitated. The refinement of unit cell
589 parameters confirmed the simultaneous incorporation of calcium and thorium within the

crystal structure. Nevertheless, the evolution of such neoformed phase as a function of leaching time underlines its meta-stability : indeed, thorium and calcium were progressively released during the chemical conversion, leading to additional phases such as $Th_2(PO_4)_2(HPO_4).H_2O$. These conclusions appear consistent with those given by Jonasson et al. who studied the solubility of some hydrated rare-earth element phosphates with implications for diagenesis and sea water concentrations (Jonasson et al. 1985). Indeed, they suggested that hydrated phosphates were important phases in controlling rare-earth element concentrations in sea waters but also noted that rhabdophane could be considered as a meta-stable phase compared to monazite.

In order to complete the description of the monazite, cheralite and monazite-cheralite solid-solution solubility close to the point of saturation, experiments with under-saturated conditions were also conducted. For this purpose, the surfaces of leached powdered or sintered samples of monazite/cheralite solid-solutions were characterized by several techniques including SEM, EPMA or grazing incidence XRD (GI-XRD). From these results, the surface of sintered altered pellets was not strongly modified compared to that of the raw materials (Figure 6). Indeed, neither preferential dissolution at grain boundaries nor the formation of corrosion pits was detected on the micrographs, which are features that were observed on other phosphate-based matrices such as β-TPD and associated solid solutions (Clavier et al. 2006). Nevertheless, a gelatinous, probably amorphous phase formed on the surface of the samples. Such observations suggested that the dissolution occurred homogeneously on grains, grains boundaries and triple junctions. It probably corresponds to the first dissolution step where the progress of the reaction was not high enough to exploit surface heterogeneities on the surface of leached samples.

The progress of the dissolution reaction was increased by conducting similar leaching tests for 3 years in 10^{-1}M HNO_3 at 90°C on Th-based cheralite sintered samples (du Fou de

615 Kerdaniel 2007). Under such experimental conditions, two phases were observed on the SEM
616 micrographs (Figure 6). The first phase was the initial $Ca_{0.5}Th_{0.5}PO_4$ cheralite, while the
617 second appeared as 1 to 10 µm aggregates exhibiting a layered morphology very similar to
618 that of thorium phosphate hydrogenphosphate hydrate (TPHPH) (Dacheux et al. 2005). The
619 small size of such grains precluded reliable EPMA-based identification. Conversely, XRD
620 analysis of the leached powder (Figure 7) confirmed the presence of TPHPH (Dacheux et al.
621 2005) as well as two small XRD lines that could be assigned to thorium hydroxophosphate
622 $Th(OH)PO_4$ (Dacheux et al. 2007a).

623 If the formation of such thorium phosphates was expected during the dissolution process
624 of Th-cheralites (Table 6), it is not likely to happen when dealing with monazite-cheralite
625 solid solutions. Indeed, in such cases, the dissolution always appeared to be congruent which
626 implies a similar behaviour for thorium and rare earth elements. On the basis of results
627 reported in literature, one can expect that thorium and lanthanide concentrations should be
628 controlled in the leachate by the precipitation of $Ln_{1-2x}Ca_xTh_x(PO_4)$. nH_2O rhabdophane.
629 Nevertheless, due to the high chemical durability of the sintered samples studied, the
630 formation of such phase onto the surface of the leached pellet was not observed directly for
631 the leaching times considered.

632

633 **Conclusion**

634

635 Several properties of monazite argue for their use as a promising specific conditioning
636 matrix for minor actinides. Among them, one can cite its structural flexibility, good response
637 to sintering, high chemical durability and resistance to radiation damage.

638 From a chemical point of view, the monazite structure allows for a large variety of cationic
639 and anionic substitutions that leads to a very broad panel of chemical composition. In this

640 structure, actinides are mainly incorporated in monazite-cheralite or monazite-huttonite solid
641 solutions through coupled $M^{III} \Leftrightarrow (M^{II}+M^{IV})$ and $(M^{III} + PO_4) \Leftrightarrow (M^{IV} + SiO_4)$ coupled mixed
642 substitutions, respectively. While wet chemistry methods, especially those involving
643 rhabdophane-type precursor precipitates can be used to promote the incorporation of trivalent
644 actinides (Am, Cm), dry chemistry routes are still favoured for tetravalent actinides (Th, U,
645 Np) incorporation. Plutonium appears to be particularly sensitive the method of preparation
646 since it can be stabilized either in the trivalent or tetravalent oxidation state. Until now, all the
647 chemical approaches to synthesis argue for the incorporation of plutonium (III) in monazite
648 rather than plutonium (IV) in cheralite or monazite-cheralite solid solutions. However, given
649 the structural flexibility of monazite, it is probably that other substitutions involving actinides
650 are available.

651 To avoid dust contamination during the handling of actinide based powders, sintering of
652 monazite and monazite/cheralite was also examined. Once again, the interesting properties of
653 this material were observed through its rather good sintering response (1350 – 1500°C). The
654 use of wet chemistry methods or very reactive precursors allowed for significantly lower
655 sintering temperatures.

656 Efficient actinide conditioning requires the ceramics to have a high resistance to aqueous
657 alteration. The study of monazite dissolution (natural, undoped or doped with actinides)
658 confirmed the geochemical observations made on natural systems. Indeed, the chemical
659 durability of the material remains very high whatever the dissolution conditions when
660 normalized dissolution rates are compared (10^{-6} g.m^{-2}.d^{-1} < $R_L(i)$ < 10^{-3} g.m^{-2}.d^{-1}), and they are
661 10^3 to 10^6 times slower than those reported for other ceramics such as britholite. The high
662 resistance of pure monazite to aqueous alteration was maintained when tetravalent actinides
663 are incorporated via the monazite-cheralite solid solution. Moreover, the very low solubility
664 of phosphate phases generally led to the precipitation of neoformed phases in the back-end of

665 the initial dissolution process. Among them, the frequent formation of rhabdophane-type
666 phases illustrates their links with monazite since they may act either as precursors during wet
667 chemistry routes or as solubility controlling phases during dissolution tests (Figure 8). In the
668 latter case, their precipitation onto the surface of the leached samples usually enhances the
669 high chemical durability, and therefore positively impacts the long term behaviour of the
670 ceramics were they to be used for long-term storage in geological repository.

671 **Acknowledgements**

672 We would like to thank S. Neumeier and G.R. Lumpkin for their fruitful comments and
673 C.J. Hetherington for his very efficient and constructive editorial work.

674

675

676 **References**

677

678 Abraham, M.M., Boatner, L.A., Quincy, T.C., Thomas, D.K. and Rappaz, M. (1980) Preparation and
679 compaction of synthetic monazite powders. Radioactive Waste Management, 1, 181–191.

680 Alonso, E., Sherman, A.M., Wallington, T.J., Everson, M.P., Field, F.R. and Roth, R. (2012)
681 Evaluating rare earth element availability : a case with revolutionary demand from clean technologies.
682 Environmental Science and Technology, 46, 3406-3414.

683 Aloy, A.S., Kovarskaya, E.N., Koltsova, T.I., Samoylov, S.E., Rovnyi, S.I., Medvedev, G.M. and
684 Jardine, L.J. (2001) Immobilization of 241-Am formed under plutonium metal conversion into
685 monazite-type ceramics, Proceedings of the 8th International Conference on Environmental
686 Management (ICEM 2001).

687 Anderson, E.B. and Burakov, B.E. (2004) Ceramics for the immobilization of plutonium and
688 americium: current progress of R&D of the V.G. Khlopin Radium Institute. Materials Research
689 Society Symposium Proceedings, 807, 207–212.

Be Mezeme, E., Cocherie, A., Faure, M., Legendre, O. and Rossi, Ph. (2006) Electron microprobe monazite geochronology of magmatic events : examples from Variscan migmatites and granitoids, Massif Central, France. Lithos, 87, 276-288.

Bjorklund, C.W. (1957) The preparation of PuP_2O_7 and $PuPO_4$. Journal of the American Chemical Society, 79, 6347-6350.

Boatner, L.A. (2002) Synthesis, structure and properties of monazite, pretulite and xenotime. Reviews in Mineralogy and Geochemistry, 48, 87-120.

Boatner, L.A., Abraham, M.M. and Rappaz, M. (1980a) Analogs of monazite for the storage of radioactive wastes. Transactions of the American Nuclear Society, 35, 186-187.

Boatner, L.A, Beall, G.W, Abraham, M.M., Finch, C.B., Huray, P.G. and Rappaz, M (1980b) Monazite and other lanthanide orthophosphates as alternate actinide waste forms. Scientific Basis for Nuclear Waste Management, 2, 289-296.

Boatner, L.A. and Sales, B.C. (1988) Monazite. Radioactive waste forms for the future, Eds Lutze, W. and Ewing, R.C., Elsevier Science Publishers B.V., 495-564.

Brandel, V. and Dacheux, N. (2004a) Chemistry of tetravalent actinide phosphates – Part I. Journal of Solid State Chemistry, 177, 4743-4754.

Brandel, V. and Dacheux, N. (2004b) Chemistry of tetravalent actinide phosphates – Part II. Journal of Solid State Chemistry, 177, 4755-4767.

Bregiroux, D., Lucas, S., Champion, E., Audubert, F. and Bernache-Assollant, D. (2006) Sintering and microstructure of rare earth phosphate ceramics $REPO_4$ with RE = La, Ce or Y. Journal of the European Ceramic Society, 26, 279-287.

Bregiroux, D., Audubert, F., Charpentier, T., Sakellariou, D. and Bernache-Assollant, D. (2007a) Solid-state synthesis of monazite-type compounds $LnPO_4$ (Ln = La to Gd). Solid State Sciences, 9, 432-439.

Bregiroux, D., Belin, R., Valenza, P., Audubert, F. and Bernache-Assollant, D. (2007b) Plutonium and americium monazite materials: Solid state synthesis and X-ray diffraction study. Journal of Nuclear Materials, 366, 52-57.

Bregiroux, D., Terra, O., Audubert, F., Dacheux, N., Serin, V., Podor, R. and Bernache-Assollant, D. (2007c) Solid-state synthesis of monazite-type compounds containing tetravalents elements. Inorganic Chemistry, 46, 10372-10382.

Bregiroux, D., Audubert, F. and Bernache-Assollant, D. (2009) Densification and grain growth during solid state sintering of $LaPO_4$. Ceramics International, 35, 1115-1120.

Burakov, B.E., Yagovkina, M.A., Garbuzov, V.M., Kitsay, A.A and Zirlin, V.A. (2004) Self-irradiation of monazite ceramics : contrasting behaviour of $PuPO_4$ and $(La,Pu)PO_4$ doped with Pu-238. Materials Research Society Symposium Proceedings, 824, 219-223.

Burnaeva, A.A., Volkov, Y.F., Kryukova, A.I., Korshunov, I.A. and Skiba, O.V. (1992) Dimorphism and crystallochemical features of sodium plutonium(IV) phosphate of the composition $NaPu_2(PO_4)_3$. Radiokhimiya, 34, 13–21.

Calestani, G. and Andretti, G.D (1984) The crystal-structure of the $Pb_{0.5}Th_{0.5}VO_4$ polymorphs with scheelite-type, zircon-type and huttonite-type structures. Zeitschrift für Kristallographie, 168, 41–51.

Cetiner, Z.S., Wood, S.A. and Gammons, C.H. (2005) The aqueous geochemistry of the rare earth elements, Part XIV : The solubility of rare earth elements phosphates from 23 to 150°C. Chemical Geology, 217, 147-169.

Cho, I.S., Choi, G.K., An, J.S., Kim, J.R. and Hong, K.S. (2009) Sintering, microstructure and microwave dielectric properties of rare earth orthophosphates $RePO_4$ (Re = La, Ce, Nd, Sm, Tb, Dy, Y, Yb). Materials Research Bulletin, 44, 173-178.

Clavier, N., Dacheux, N., Martinez, P., du Fou de Kerdaniel, E., Aranda, L. and Podor, R. (2004) Sintering of β-Thorium-Uranium(IV) Phosphate-Diphosphate solid solutions from low-temperature precursors. Chemistry of Materials, 16, 3357-3366.

739 Clavier, N., Dacheux, N. and Podor, R. (2006a) Synthesis, characterization, sintering and leaching of
740 β-TUPD/monazite radwaste matrices. Inorganic Chemistry, 45, 220-229.

741 Clavier, N., du Fou de Kerdaniel, E., Dacheux, N., Le Coustumer, P., Drot, R., Ravaux, J. and Simoni,
742 E. (2006b) Behavior of thorium-uranium(IV) phosphate-diphosphate sintered samples during leaching
743 tests, Part II : Saturation processes. Journal of Nuclear Materials, 349, 304-316.

744 Clavier, N., Dacheux, N., Wallez, G. and Quarton, G. (2007) Hydrothermal methods as a new way of
745 actinide phosphate preparation. Materials Research Society Symposium Proceedings, 985, 169-174.

746 Clavier, N., Podor, R. and Dacheux, N. (2011) Crystal chemistry of the monazite structure. Journal of
747 the European Ceramic Society, 31, 941-976.

748 Cuney, M. and Mathieu, R. (2000) Extreme light rare earth element mobilization by diagenetic fluids
749 in the geological environment of the Oklo natural reactor zones, Franceville basin, Gabon. Geology,
750 28, 743-746.

751 Dacheux, N., Chassigneux, B., Brandel, V., Le Coustumer, P., Genet, M. and Cizeron, G. (2002)
752 Reactive sintering of the thorium phosphate-diphopshate : Study of physical, thermal, and
753 thermomechanical properties and chemical durability during leaching tests. Chemistry of Materials,
754 14, 2953-2961.

755 Dacheux, N., Clavier, N., Robisson, A.C., Terra, O., Audubert, F., Lartigue, J.E. and Guy, C. (2004)
756 Immobilisation of actinides in phosphate matrices. Comptes Rendus Chimie, 7, 1141-1152.

757 Dacheux, N., Clavier, N., Wallez, G., Brandel, V., Emery, J., Quarton, M. and Genet, M. (2005)
758 Characterization of the thorium phosphate-hydrogenphosphate hydrate (TPHPH) and study of its
759 transformation into the thorium phosphate-diphopshate (β-TPD). Materials Research Bulletin, 40,
760 2225-2242.

761 Dacheux, N., Clavier, N. and Ritt, J. (2006) Behavior of thorium-uranium (IV) phosphate-diphosphate
762 sintered samples during leaching tests, Part I : Kinetic study. Journal of Nuclear Materials, 349, 291-
763 303.

764 Dacheux, N., Clavier, N., Wallez, G. and Quarton, M. (2007a) Crystal structures of $Th(OH)PO_4$,
765 $U(OH)PO_4$ and $Th_2O(PO_4)_2$. Condensation mechanism of $M^{IV}(OH)PO_4$ (M = Th, U) into $M_2O(PO_4)_2$.
766 Solid State Sciences, 9, 619-627.

767 Dacheux, N., Grandjean, S., Rousselle, J. and Clavier, N. (2007b) Hydrothermal way of preparation of
768 actinides (IV) phosphate hydrogenphosphate hydrates and study of their conversion into actinides (IV)
769 phosphate diphosphate solid solutions. Inorganic Chemistry, 46, 10390-10399.

770 Dacheux, N., du Fou de Kerdaniel, E., Clavier, N., Podor, R., Aupiais, J. and Szenknect, S. (2010)
771 Kinetics of dissolution of thorium and uranium doped britholite ceramics. Journal of Nuclear
772 Materials, 404, 33-43.

773 Davis, D.D., Vance, E.R. and McCarthy, G.J. (1981) Crystal chemistry and phase relations in the
774 synthetic minerals of ceramic waste forms. II : studies of uranium-containing compounds. Scientific
775 Basis for Nuclear Waste Management, 3, 197-200.

776 Deberdt, S., Castet, S., Dandurand, J.L., Harrchoury, J.C. and Louiset, I. (1998) Experimental study of
777 $La(OH)_3$ and $Gd(OH)_3$ solubilities (25 to 150°C), and La-acetate complexing (25 to 80°C). Chemical
778 Geology, 151, 349-372.

779 Deschanels, X., Picot, V., Glorieux, B., Jorion, F., Peuget, S., Roudil, D., Jegou, C., Broudic. V;,
780 Cachia, J.N., Advocat, T., Den Auwer, C., Fillet, C., Coutures, J.P., Hennig, C., Scheinost, A. (2006)
781 Plutonium incoporation in phosphate and titanate ceramics for minor actinide containment. Journal of
782 Nuclear Materials, 352, 233-240.

783 Drozdzynski, J. (1979) Methods of preparation of uranium (+3) compounds from solutions. Inorganica
784 Chimica Acta, 32, 83-85.

785 du Fou de Kerdaniel, E. (2007) Etude de la dissolution de britholites et de solutions solides
786 monazite/brabantite dopées avec des actinides. Ph. D. of the Université Paris-Sud-11, IPNO-T-08-02
787 (in french).

du Fou de Kerdaniel, E., Clavier, N., Dacheux, N., Terra, O. and Podor, R. (2007) Actinide solubility-controlling phases during the dissolution of phosphate ceramics. Journal of Nuclear Materials, 362, 451-458.

El-Nadi, Y.A., Daoud, J.A. and Aly, H.F. (2005) Modified leaching and extraction of uranium from hydrous oxide cake of Egyptian monazite. International Journal of Mineral Processing, 76, 101-110.

Eyal, Y. and Kaufman, A. (1982) Alpha recoil damage in monazite – Preferential dissolution of the radiogenic actinide isotopes. Nuclear Technology, 58, 77-83.

Eyal, Y. and Olander, D.R. (1990) Leaching of uranium and thorium from monazite: I. Initial leaching. Geochimica et Cosmochimica Acta, 54, 1867-1877.

Ewing, R.C. (2007) Ceramic matrices for plutonium disposition. Progress in Nuclear Energy, 49, 635-643.

Ewing, R.C. and Haaker, R.F. (1980) The metamict state : implications for radiation damage in crystalline waste forms. Nuclear and Chemical Waste Management, 1, 51-57.

Ewing, R.C., Lutze, W. and Weber, W.G. (1995) Zircon – a host phase for the disposal of weapons plutonium. Journal of Materials Research, 10, 243-246.

Ewing, R.C. and Wang, L.M. (2002) Phosphate as nuclear waste form. Reviews in Mineralogy & Geochemistry, 48, 673-699.

Förster, H.J. (1998) The chemical composition of REE-Y-Th-U-rich accessory minerals in peraluminous granites of the Erzgebirge-Fichtelgebirge region, Germany. Part I : the monazite-(Ce)-brabantite solid solution series. American Mineralogist, 83, 259-272.

Förster, H.J. and Harlov, D.E. (1999) Monazite-(Ce)-huttonite solid solutions in granulite-facies metabasites from the Ivrea-Verbano zone, Italy. Mineralogical Magazine, 63, 587-594.

Furrer, G. and Stumm, W. (1986) The coordination chemistry of weathering. 1. Dissolution kinetics of δ-Al_2O_3 and BeO. Geochimica et Cosmochimica Acta, 50, 1847-1860.

Ganor, J., Mogollon, J.L. and Lasaga, A.C. (1995) The effect of pH on kaolinite dissolution rates and on activation energy. Geochimica et Cosmochimica Acta, 59, 1037-1052.

Glorieux, B., Montel, J.M. and Matecki, M. (2009) Synthesis and sintering of a monazite-brabantite solid solutions ceramics using metaphosphate. Journal of the European Ceramic Society, 29, 1679-1686.

Goyne, K.W., Brantley, S.L. and Chorover, J. (2010) Rare earth element release from phosphate minerals in the presence of organic acids. Chemical Geology, 278, 1-14.

Gramaccioli, C.M. and Segalstad, T.M. (1978) Uranium-rich and thorium-rich monazite from a south-alpine pegmatite at Piona, Italy. American Mineralogist, 63, 757-761.

Guy, C., Audubert, F., Lartigue, J.E., Latrille, C., Advocat, T. and Fillet, C. (2002) New conditionings for separated long-lived radionuclides. Comptes Rendus Physique, 3, 827-837.

Haire, R.G., Hellwege, H.E., Hobart, D.E. and Young, J.P. (1983) Syntheses, lattice parameters and solid state absorption spectra of the first transplutonium orthophosphates. Journal of the Less Common Metals, 93, 358-359.

Heisbourg, G., Hubert, S., Dacheux, N. and Ritt, J. (2003) The kinetics of dissolution of $Th_{1-x}U_xO_2$ solid solutions in nitric media. Journal of Nuclear Materials, 321, 141-151.

Heisbourg, G., Hubert, S., Dacheux, N. and Purans, J. (2004) Kinetic and thermodynamic studies of the dissolution of thoria-urania solid solutions. Journal of Nuclear Materials, 335, 5-13.

Helean, K.B., Lutze, W. and Ewing, R.C. (1999) Dissolution studies of inert materials. Ceramic Transactions, 93, 357-363.

Hernandez, T. and Martin, P. (2008) Effect of the phosphorous/cerium ratio in the properties of sintered Ce-monazite. Journal of Alloys and Compounds, 466, 568-575.

Hetherington, C.J. and Harlov, D. (2008) Metasomatic thorite and uraninite inclusions in xenotime and monazite from granitic pegmatites, Hidra anorthosite massif, southwestern Norway : Mechanics and fluid chemistry. American Mineralogist, 93, 806-820.

Hikichi, Y., Hukuo, K. and Shiokawa, J. (1978) Solid solutions in the systems monazite ($CePO_4$) - huttonite ($ThSiO_4$) and monazite - $(Ca_{0.5}Th_{0.5})PO_4$. Nippon Kagaku Kaishi, 12, 1635-1640 (in Japanese).

Hobart, D.E., Begun, G.M., Haire, R.G. and Hellwege, H.E. (1983) Raman spectra of the transplutonium orthophosphates and trimetaphosphates. Journal of Raman Spectroscopy, 14, 59–62.

Horlait, D., Clavier, N., Szenknect, S., Dacheux, N. and Dubois, V. (2012a) Dissolution of cerium(IV)-lanthanide(III) oxides: comparative effect of chemical composition, temperature, and acidity. Inorganic Chemistry, 51, 3868-3878.

Horlait, D., Tocino, F., Clavier, N., Dacheux, N., Szenknect, S. (2012b) Multiparametric study of $Th_{1-x}Ln_xO_{2-x/2}$ mixed oxides dissolution in nitric acid media. Journal of Nuclear Materials, 429, 237-244.

Hutton, C.O. (1951) Occurrence, optical properties and chemical composition of huttonite. American Mineralogist, 36, 66-69.

Jonasson, R.G., Bancroft, G.M. and Nesbitt, H.W. (1985) Solubilities of some hydrous REE phosphates with implications for diagenesis and sea-water concentrations. Geochimica et Cosmochimica Acta, 49, 2133-2139.

Kamel, N.H., Khadoudja, R., Arabi, M., Kamel, Z., Zahri, A. and Metahri, S. (2010) Effect of the synthesis method on the properties of a Pb-bearing (Y-Gd-Ce) rare-earth phosphate used for the confinement of high-level radioactive waste. Journal of Nuclear Materials, 401, 104-112.

Karioris, F.G., Gowda, K.A. and Cartz, L. (1981) Heavy-ion bombardment of monoclinic $ThSiO_4$, ThO_2 and monazite. Radiation Effects Letters, 67, 83-85.

Keller, C. (1963) Untersuchung über die Germinate und Silicate des Types ABO4 der vierwertigen Elemente Thorium bis Americium. Nukleonika, 5, 41-48 (in german).

Keller, C. and Walter, K.H. (1965) Darstellung, Gitterkonstanten und chemische Eigenschaften einiger ternärer Oxide des Plutoniums, Americiums und Curiums vom Typ $Me^{III}_XVO_4$. Journal of Inorganic and Nuclear Chemistry, 27, 1253-1260 (in german).

Kelly, K.L., Beall, G.W., Young, J.P., Boatner, L.A. (1980) Valence states of actinides in synthetic monazites. Scientific Basis for Nuclear Waste Management, 3, 189-195.

Krenn, E., Ustaszewski, K., Finger, F. (2008) Detrital and newly formed metamorphic monazite in amphibolite-facies metapelites from the Motajica Massif, Bosnia. 254, 164-174.

King, E.L. (1949) The solubility of plutonium(IV) phosphates and the phosphate complexes of plutonium(IV). The Transuranium Elements, Eds. Seaborg, G.T., Katz, J.J., Manning, W.M., 638-665.

Kitaev, D.B., Volkov, Y.F. and Orlova, A.I. (2004) Orthophosphates of tetravalent Ce, Th, U, Np and Pu with the monazite structure. Radiochemistry, 46, 211-217.

Kitsay, A.A., Garbuzov, V.M. and Burakov, B.E. (2004) Synthesis of actinide-doped ceramics: from laboratory experiments to industrial scale technology. Materials Research Society Symposium Proceedings, 807, 237-242.

Krauskopf, K.B. (1986) Thorium and rare-earth metals as analogs for actinide elements. Chemical Geology, 55, 323-335.

Kucha, H. (1980) Continuity in the monazite-huttonite series. Mineralogical Magazine, 43, 1031-1034.

Lasaga, A.C. (1998) Kinetic theory in the earth sciences. Princeton University Press, Princeton.

Leonardos, O.H. (1974) Origin and provenance of fossil and recent monazite deposits in Brazil. Economic Geology, 69, 1126-1128.

Leturcq, G., Advocat, T., Hart, K., Berger, G., Lacombe, J. and Bonnetier, A. (2001) Solubility study of Ti,Zr-based ceramics designed to immobilize long-lived radionuclides. American Mineralogist, 86, 871-880.

Linthout, K. (2007) Tripartite division of the system $2REEPO_4 - CaTh(PO_4)_2 - 2ThSiO_4$, discreditation of brabantite, and recognition of cheralite as the name for members dominated by $CaTh(PO_4)_2$. The Canadian Mineralogist, 45, 503-508.

Lumpkin, G.R. (1998) Rare element mineralogy and internal evolution of the Rutherford #2 pegmatite, Amelia County, Virginia; a classic locality revisited. The Canadian Mineralogist, 36, 339-353.

Lumpkin, G.R., Geisler-Wierwille, T. (2012) Ceramic Waste Forms, in Comprehensive Nuclear Materials, Vol. 5 : Material performance and corrosion / Waste materials, Eds. R.J.M. Konings, T.R. Allen, R.E. Stoller, S. Yamanaka, Elsevier (Amsterdam), 563-600.

Meldrum, A., Boatner, L.A., Weber, W.J. and Ewing, R.C. (1998) Radiation damage in zircon and monazite. Geochimica et Cosmochimica Acta, 62, 2509-2520.

Montel, J.M., Kornprobst, J. and Vielzeuf, D. (2000) Preservation of old U-Th-Pb ages in shielded monazite : example from the Beni Bousera hercyninan kinzigites (Morocco). Journal of Metamorphic Geology, 18, 335-342.

Montel, J.M., Glorieux, B., Seydoux-Guillaume A.M. and Wirth, R. (2006) Synthesis and sintering of monazite-brabantite solid solution ceramic for nuclear waste storage. Journal of Physics and Chemistry of Solids, 67, 2489-2500.

Montel, J.M., Razafimahatratra, D., Ralison, B., De Parseval, P., Thibault, M. and Randranja, R. (2011) Monazite from mountain to ocean : a case study from Trolognaro (Fort-Dauphin), Madagascar. European Journal of Mineralogy, 23, 745-757.

Morgan, P.E.D., Housley, R.M., Davis, J.B., DeHaan, M.L. and Marshall, D.B. (2005) Chemical and ceramic methods towards the safe storage of actinides. DOE Report DOE/ER/45617.

Muto, T., Merowitz, R., Pommer, A.M. and Murano, T.J. (1959) Ningyoite, a new uranous phosphate mineral from Japan. American Mineralogist, 44, 633-650.

Myasoedov, B.F., Kirby, H.W. and Tananaev, I.G. (2006) The chemistry of the actinide and transactinide elements. Springer, Dordrecht.

Nabar, M.A. and Mhatre, B.G. (1987) Studies on triple orthovanadates: IV. Crystal chemistry of the solid solutions $Ca_{1-x}Ba_xLaTh(VO_4)_3$. Inorganica Chimica Acta, 140, 165-166.

912 Nabar, M.A. and Mhatre, B.G. (2001) Studies on triple orthovanadates. VIII. Synthesis and
913 spectrostructural characterization of triple orthovanadates $BaLnTh(VO_4)_3$ (Ln = La or Pr) and
914 $BaLnCe(VO_4)_3$ (Ln = La, Pr, Nd or Sm). Journal of Alloys and Compounds 323-324, 83-85.

915 Nabar, M.A. and Sakhardande, R.R. (1985) Monazite to scheelite transition in $CdNdTh(AsO_4)_3$.
916 Journal of the Less Common Metals, 110, 415-420.

917 Nabar, M.A. and Sakhardande, R.R. (1999) Studies on thorium containing triple orthoarsenates:
918 $MRETh(AsO_4)_3$ (M = Mg, Sr, Ba, Cd and Pb, RE = La, Pr, Nd, Sm, Gd, Tb, Dy and Y). Journal of
919 Alloys and Compounds, 285, 82-84.

920 Ni, Y.X., Hugues, J.M. and Mariano, A.N. (1995) Crystal chemistry of the monazite and xenotime
921 structures. American Mineralogist, 80, 21-26.

922 Oelkers, E.H. and Poitrasson, F. (2002) An experimental study of the dissolution stoichiometry and
923 rates of a natural monazite as a fuction of temperature from 50 to 230°C and pH from 1.5 to 10.
924 Chemical Geology, 191, 73-87.

925 Olander, D.R.and Eyal, Y. (1990a) Leaching of uranium and thorium from monazite: II. Elemental
926 leaching. Geochimica et Cosmochimica Acta, 54, 1879-1887.

927 Olander, D.R.and Eyal, Y. (1990b) Leaching of uranium and thorium from monazite: III. Leaching of
928 radiogenic daughters. Geochimica et Cosmochimica Acta, 54, 1889-1896.

929 Overstreet, W.C. (1967) The geological occurrence of monazite. U.S. Geological Surv. Prof. Paper,
930 530.

931 Paquette, J.L., Goncalves, P., Devouard, B., Nicollet, C. (2004) Mico-drilling ID-TIMS U-Pb dating
932 of single monazites: a new method to unravel complex poly-metamorphic evolutions. Application to
933 the UHT granulites of Andriamena (North-Central Madagascar). Contributions to Mineralogy and
934 Petrology, 147, 110-122.

935 Pepin, G.J., Vance, E.R. and McCarthy, G.J. (1981) The crystal-chemistry of cerium in the monazite
936 structure-type phase of tailored-ceramic nuclear waste forms. Materials Research Bulletin, 16, 627-
937 633.

Picot, V., Deschanels, X., Peuget, S., Glorieux, B., Seydoux-Guillaume, A.M., Wirth, R. (2008) Ion beam irradiation effects in monazite, 381, 290-296.

Podor, R. (1994) Synthèse et caractérisation des monazites uranifères et thorifères. Ph. D. of the Université Henri Poincaré Nancy I (in french).

Podor, R. and Cuney, M. (1997) Experimental study of Th-bearing $LaPO_4$ (780°C, 200MPa) : implications for monazite and actinide orthophosphate stability. American Mineralogist, 82, 765-771.

Podor, R., Cuney, M. and Nguyen-Trung, C. (1995) Experimental study of the solid solution between monazite-(La) and $(Ca_{0.5}U_{0.5})PO_4$ at 780°C and 200 MPa. American Mineralogist, 80, 1261-1268.

Podor, R., François, M. and Dacheux, N. (2003). Synthesis, characterization, and structure determination of the orthorhombic $U_2(PO_4)(P_3O_{10})$. Journal of Solid State Chemistry, 172, 66-72.

Pointeau, V., Deditius, A.P., Miserque, F., Renock, D., Becker, U., Zhang, J., Clavier, N., Dacheux, N., Poinssot, C. and Ewing, R.C. (2009) Synthesis and characterization of coffinite. Journal of Nuclear Materials, 393, 449-458.

Poitrasson, F., Chenery, S. and Shepherd, T.J. (2000) Electron microprobe and LA-ICP-MS study of monazite hydrothermal alteration : implications for U-Th-Pb geochronology and nuclear ceramics. Geochimica et Cosmochimica Acta, 64, 3283-3297.

Poitrasson, F., Oelkers, E., Schott, J. and Montel, J.M. (2004) Experimental determination of synthetic $NdPO_4$ monazite end-member solubility in water from 21°C to 300°C : implications for rare earth element mobility in crustal fluids. Geochimica et Cosmochimica Acta, 68, 2207-2221.

Pokrovsky, O.S. and Schott, J. (2000) Kinetics and mechanism of forsterite dissolution at 25°C and pH from 1 to 12. Geochimica et Cosmochimica Acta, 64, 3313-3325.

Polyakov, E.V., Volkov, I.V., Surikov, V.T., Perelyaeva, L.A. and Shveikin, G.P. (2009) Behavior of monazite components in humic acid solutions. Doklady Chemistry, 428, 242-245.

Popa, K., Colineau, E., Wastin, F. and Konings, R.J.M. (2007) The low-temperature heat capacity of $(Pu_{0.1}La_{0.9})PO_4$. Solid State Communications, 144, 74-77.

963 Popa, K., Wallez, G., Raison, P.E., Bregiroux, D., Apostolidis, C., Lindqvist-Reis, P. and Koning,
964 R.J.M. (2010) $SrNp(PO_4)_2$: an original ordered modification of cheralite. Inorganic Chemistry, 49,
965 6904-6908.

966 Pourtier, E., Devidal, J.L. and Gibert, F. (2010) Solubility measurements of synthetic neodymium
967 monazite as a function of temperature at 2 kbars, and aqueous neodymium speciation in equilibrium
968 with monazite. Geochimica et Cosmochimica Acta, 74, 1872-1891.

969 Rai, D., Felmy, A.R. and Fulton, R.W. (1992) Solubility and ion activity product of $AmPO_4.xH_2O$.
970 Radiochimica Acta, 56, 7-14.

971 Raison, P.E., Jardin, R., Bouexiere, D., Konings, R.J.M., Geisler, T., Pavel, C.C. and Rebizant, J.
972 (2008) Structural investigation of the synthetic $CaAn(PO_4)_2$ (An = Th and Np) cheralite-like
973 phosphates. Physics and Chemistry of Minerals, 35, 603-609.

974 Rajesh, K., Sivakumar, B., Krishna Pillai, P., Mukundan, P., Warrier, K.G.K. and Nair, V.R. (2004)
975 Synthesis of nanocrystalline lanthanum phosphate for low-temperature densification to monazite
976 ceramics. Materials Letters, 58, 1687-1691.

977 Ranney, T.A. and Parker, L.V. (1998) Comparison of fiberglass and other polymeric well casings, part
978 III. Sorption and leaching of trace-level metals. Ground Water Monitoring and Remediation, 18, 127-
979 133.

980 Rapp, R.P. and Watson, E.B. (1986) Monazite solubility and dissolution kinetics – Implications for the
981 thorium and light rare-earth chemistry of felsic magmas. Contributions to Mineralogy and Petrology,
982 94, 304-316.

983 Rasmussen, B., Fletcher, I.R., Muhling, J.R., Wilde, S.A. (2010). In situ U-Th-Pb geochronology of
984 monazite and xenotime from the Jack Hills belt: implications for the age of deposition and
985 metamorphism of Hadean zircons. Precambrian Research, 180, 26-46.

986 Rasmussen, B., Fletcher, I.R., Muhling, J.R. (2007). In situ U-Pb dating and element mapping of three
987 generations of monazite: unravelling crytic tectonothermal events in low-grade terranes. Geochimica
988 et Cosmochimica Acta, 71, 670-690.

Read, D. (2002) The degradation of monazite : implications for the mobility of rare-earth and actinide elements during low-temperature alteration. European Journal of Mineralogy, 14, 487-498.

Robisson, A.C., Dacheux, N. and Aupiais, J. (2002) Influence of the pH on the dissolution of TPD and associated solid solutions. Journal of Nuclear Materials, 306, 134-146.

Rose, D. (1980) Brabantite, $CaTh(PO_4)_2$, a new mineral of the monazite group. Neues Jahrbuch für Mineralogie - Monatshefte, H(6), 247-257.

Rovnyi, S.I., Medvedev, G.M., Aloy, A.S., Koltsova, T.I. and Samoylov, S.E. (2004) REE and TRU incorporation into monazite structure ceramics. Materials Research Society Symposium Proceedings, 824, 237-241.

Roy, R. and Vance, E.R. (1981) Irradiated and metamict materials – Relevance to radioactive waste science. Journal of Materials Science, 16, 1187-1190.

Sales, B.C., White, C.W. and Boatner, L.A. (1983) A comparison of the corrosion characteristics of synthetic monazite and borosilicate glass containing simulated nuclear defense waste. Nuclear and Chemical Waste Management, 4, 281-289.

Sandino, A. and Bruno, J. (1992) The solubility of $(UO_2)_3(PO_4)_2.4H_2O$ and the formation of U(VI) phosphate complexes – Their influence in uranium speciation in natural-waters. Geochimica et Cosmochimica Acta, 56, 4135-4145.

Schmidt, C., Rickers, K., Bilderback, D.H. and Huang, R. (2007) In situ synchrotron radiation XRF study of REE phosphate dissolution in aqueous fluids to 800°C. Lithos, 95, 87-102.

Seydoux-Guillaume, A.M., Paquette, J.L., Wiedenbeck, M., Montel, J.M., Heinrich, H. (2002) Experimental resetting of the U-Th-Pb systems in monazite. Chemical Geology, 191, 165-181.

Sillen, L.G. and Martell, A.E. (1964) Stability constants of metal ligand complexes. Eds. The Chemical Society special publication n°17, London : Burlington House.

Slodowska-Curie, M. (1898) Rayons émis par les composés de l'uranium et du thorium. Compte-Rendus Académie des Sciences Paris, 126, 1101-1103 (in french).

Speer, J.A. (1980) The actinide orthosilicates. Reviews in Mineralogy and Geochemistry, 5, 113-135.

Tabuteau, A., Pages, M., Livet, J. and Musikas, C. (1988) Monazite-like containing trans-uranium elements (neptunium and plutonium). Journal of Materials Science Letters, 7, 1315-1317

Tamain, C., Ozgumus, A., Dacheux, N., Garrido, F. and Thomé, L. (2006) Effects of irradiation on the thorium phosphate-diphosphate ceramics (β-TPD) and consequences on its dissolution. Journal of Nuclear Materials, 352, 217-223.

Tamain, C., Dacheux, N., Garrido, F. and Thomé, L. (2007) Irradiation effects on thorium phosphate diphosphate : Chemical durability and thermodynamic study. Journal of Nuclear Materials, 362, 459-465.

Terra, O., Clavier, N., Dacheux, N. and Podor, R. (2003) Preparation and characterization of lanthanum-gadolinium monazites as ceramics for radioactive waste storage. New Journal of Chemistry, 27, 957-967.

Terra, O., Dacheux, N., Audubert, F. and Podor, R. (2006) Immobilization of tetravalent actinides in phosphate ceramics. Journal of Nuclear Materials, 352, 224-232.

Thomas, A.C., Dacheux, N., Le Coustumer, P., Brandel, V. and Genet, M. (2001) Kinetic and thermodynamic studies of the dissolution of thorium-uranium (IV) phosphate-diphosphate solid solutions, Journal of Nuclear Materials, 295, 249-264.

Tropper, P., Manning, C.E. and Harlov, D.E. (2011) Solubility of $CePO_4$ monazite and YPO_4 xenotime in H_2O and H_2O-NaCl at 800°C and 1 GPa : implications for REE and Y transport during high-grade metamorphism. Chemical Geology, 282, 58-66.

Vance, E.R., Zhang, Y., McLeod, T. and Davis, J. (2011) Actinide valences in xenotime and monazite. Journal of Nuclear Materials, 409, 221-224.

Vance, E.R. (2012) Ceramic Waste Forms, in Comprehensive Nuclear Materials, Vol. 5 : Material performance and corrosion / Waste materials, Eds. R.J.M. Konings, T.R. Allen, R.E. Stoller, S. Yamanaka, Elsevier (Amsterdam), 485-503

1039 Van Emden, B., Thornber, M.R., Graham, J. and Lincoln F.J. (1997) The incorporation of actinides in
1040 monazite and xenotime from placer deposits in Western Australia. The Canadian Mineralogist, 35, 95-
1041 104.

1042 Veilly, E., du Fou de Kerdaniel, E., Roques, J., Dacheux, N. and Clavier, N. (2008) Comparative
1043 behavior of britholites and monazite/brabantite solid solutions during leaching tests : a combined
1044 experimental and DFT approach. Inorganic Chemistry, 47, 10971-10979.

1045 Volkov, Y.F., Tomilin, S.V., Lukinykh, A.N., Lizin, A.A., Orlova, A.I. and Kitaev, D.B. (2002)
1046 Synthesis and X-ray diffraction study of mixed-metal orthophosphates with $NaZr_2(PO_4)_3$ and $CePO_4$
1047 structures. Radiochemistry, 44, 319-325.

1048 Walther, J.V. (1996) Relation between rates of aluminosilicate mineral dissolution, pH, temperature,
1049 and surface charge. American Journal of Science, 296, 693-728.

1050 Wintergerst, M., Dacheux, N., Datcharry, F., Herms, E. and Kapusta, B. (2009) Corrosion of the
1051 AlFeNi alloy used for the fuel cladding in the Jules Horowitz research reactor. Journal of Nuclear
1052 Materials, 393, 369-380.

1053 Zhang, Y. and Vance, E.R. (2008) Plutonium in monazite and brabantite: diffuse reflectance
1054 spectroscopy study. Journal of Nuclear Materials, 375, 311-314.

1055

1056 **Figure Caption**

1057

1058 **Figure 1.** Representation of the monazite structure (a) (after Ni et al. 1995) and LnO_9
1059 polyhedrons connection (b).

1060 **Figure 2.** SEM micrographs of $Ca_{0.5}Th_{0.4}U_{0.1}PO_4$ (a) and $Ca_{0.5}Th_{0.2}U_{0.3}PO_4$ (b) pellets
1061 sintered at 1300°C for 10 hours.

1062 **Figure 3.** Determination of $R_{L,0}$ and $R_{L,t}$ values during static and dynamic dissolution
1063 tests (inspired from Dacheux et al. 2010).

1064 **Figure 4.** Evolution of normalized weigth loss during the dissolution of $Ca_{0.5}Th_{0.4}U_{0.1}PO_4$
1065 ($N_L(Th)$ (■), $N_L(U)$ (●)) at T = 90°C (10^{-1}M HNO_3) (a) and variation of $N_L(U)$
1066 versus square root of time (b), revealing the apparition of diffusion phenomena
1067 (Lasaga 1998).

1068 **Figure 5.** Evolution of $N_L(U)$ normalized weight losses during the dissolution of
1069 $Ca_{0.5}Th_{0.3}U_{0.2}PO_4$, $Ca_{0.5}Th_{0.4}U_{0.1}PO_4$, $Ca_{0.5}Th_{0.2}U_{0.3}PO_4$ samples and of
1070 $Ca_{0.5}Th_{0.1}U_{0.4}PO_4$ in 10^{-1}M HNO_3 (T = 70°C).

1071 **Figure 6.** SEM micrographs of leached $Ca_{0.5}Th_{0.5}PO_4$ pellets (a : 10^{-1}M HNO_3 and T =
1072 90°C; b : 10^{-1}M HCl and T = 70°C) and powder (c,d : 10^{-1}M HNO_3 and
1073 T = 90°C, t = 3 years)

1074 **Figure 7.** XRD pattern of $Ca_{0.5}Th_{0.5}PO_4$ powdered sample altered during 3 years in
1075 10^{-1}M HNO_3 (T = 90°C). XRD lines of initial cheralite (**x**), TPHPH (+) and
1076 $Th(OH)PO_4$ (♠).

1077 **Figure 8.** Links between rhabdophane and monazite during heat treatment or leaching
1078 steps (after Clavier et al. 2007).

1079

1080

Table 1. Incorporation of tetravalent actinides in the monazite structure through the "cheralitic coupled substitution". Green cells indicate successful attempts while orange corresponds to failed ones. No data was reported yet for the grey-colored couples.

		M^{II}					
		Mg	Ca	Sr	Cd	Ba	Pb
An^{IV}	Th	**Yes**	**Yes**	**Yes**	**Yes**	**Yes**	**Yes**
	U	**Yes**	**Yes**	**Yes**			
	Np		**Yes**	**No**			
	Pu		**No**				

Table 2. Reported possibilities of incorporation of actinides in the monazite structure. W stands for wet chemistry methods of preparation, D for dry chemistry routes and N for Natural analogues.

	Th	**U**		**Pa**	**Np**	**Pu**		**Am – Cm**	**Bk – Es**
	IV	**III**	**IV**	**IV**	**IV**	**III**	**IV**	**III**	**III**
$An^{III}PO_4$		**W?**				**W/D**		**W/D**	**W**
$M^{II}_{0.5}An^{IV}_{0.5}PO_4$	**W/D/N**		**D/N**		**D**		**D?**		
$Ln^{III}_{1-x}An^{IV}_x(PO_4)_{1-x}(SiO_4)_x$	**N**		**N**						
$An^{IV}SiO_4$	**W/D/N**			**W**					
$An^{III}AsO_4$						**W**		**W**	**W**
$M^{II}Ln^{III}An^{IV}(AsO_4)_3$	**D**								

W? : doubtful based on the very low stability of U(III) in phosphate media

D? : Pu(IV) incorporation only obtained simultaneously to that of Np(IV) (Tabuteau et al. 1988)

1092 **Table 3.** Normalized dissolution rates determined for monazite-cheralite solid solutions in various acidic media (T = 70°C) and comparison
1093 with data reported for $LnPO_4$ monazites.

			R_L (i) ($g.m^{-2}.d^{-1}$)			Reference
		pH	Th	U	Ln	
$Ca_{0.5}Th_{0.4}U_{0.1}PO_4$	$R_{L,0}$	1	N.D.	$(9.7 \pm 0.8) \times 10^{-5}$	---	Veilly et al. 2008
		1	N.D.	$(1.3 \pm 0.1) \times 10^{-3}$	---	
$Ca_{0.5}Th_{0.3}U_{0.2}PO_4$	$R_{L,0}$	3	$(8.9 \pm 0.9) \times 10^{-4}$	N.D.	---	du Fou de Kerdaniel 2007
		4	N.D.	$(6.0 \pm 0.6) \times 10^{-4}$	---	
$Ca_{0.5}Th_{0.2}U_{0.3}PO_4$	$R_{L,0}$	1	N.D.	$(4.6 \pm 0.5) \times 10^{-3}$	---	Veilly et al. 2008
	$R_{L,t}$		N.D.	$(1.4 \pm 0.1) \times 10^{-3}$	---	
	$R_{L,0}$	3	N.D.	$(1.9 \pm 0.2) \times 10^{-3}$	---	du Fou de Kerdaniel 2007
$Ca_{0.5}Th_{0.1}U_{0.4}PO_4$	$R_{L,0}$	1	N.D.	$(2.4 \pm 0.2) \times 10^{-3}$	---	Veilly et al. 2008
	$R_{L,t}$		N.D.	$(1.8 \pm 0.2) \times 10^{-3}$	---	
	$R_{L,0}$	4	N.D.	$(1.1 \pm 0.1) \times 10^{-3}$	---	du Fou de Kerdaniel 2007
	$R_{L,t}$		N.D.	$(3.1 \pm 0.3) \times 10^{-4}$	---	
$La_{0.50}Ca_{0.25}Th_{0.15}U_{0.10}PO_4$	$R_{L,0}$	1	N.D.	$(1.7 \pm 0.2) \times 10^{-3}$	N.D.	Veilly et al. 2008
	$R_{L,t}$		N.D.	$(7.9 \pm 0.8) \times 10^{-4}$	N.D.	
	$R_{L,0}$	2	N.D.	$(1.6 \pm 0.1) \times 10^{-3}$	N.D.	du Fou de Kerdaniel 2007
	$R_{L,t}$		N.D.	$(5.0 \pm 0.5) \times 10^{-4}$	N.D.	
	$R_{L,0}$	3	N.D.	$(3.5 \pm 0.4) \times 10^{-4}$	N.D.	
	$R_{L,0}$	4	N.D.	$(3.9 \pm 0.4) \times 10^{-4}$	N.D.	
Natural monazite (Ln = Ce)	---	1	---	---	6×10^{-4}	Oelkers and Poitrasson 2002
	---	2	---	---	$2 - 3.2 \times 10^{-5}$	
	---	2.6	---	---	7×10^{-6}	
	---	6	---	---	8×10^{-7}	
$GdPO_4$	---	1	---	---	$(3.8 \pm 0.8) \times 10^{-4}$	Terra et al. 2003 (T = 90°C)
	---	4	---	---	$(4.8 \pm 1.4) \times 10^{-6}$	

1094 **Table 4.** Normalized leaching rates of cheralite and monazite-cheralite solid solutions leached in static
1095 conditions (HNO_3, T = 90°C).
1096

		pH	$R_L(i)$ ($g.m^{-2}.d^{-1}$)			
			Th	U	La	Eu
$Ca_{0.5}Th_{0.4}U_{0.1}PO_4$	$R_{L,0}$	1	< L.D.	$(2.4 \pm 0.2) \times 10^{-4}$	---	---
	$R_{L,t}$			$(2.5 \pm 0.3) \times 10^{-5}$		
$Ca_{0.5}U_{0.5}PO_4$	$R_{L,0}$	4	---	$(4.2 \pm 0.4) \times 10^{-6}$	---	---
$La_{0.4}Eu_{0.1}Ca_{0.25}Th_{0.25}PO_4$	$R_{L,0}$	1	< L.D.	---	$(1.7 \pm 0.2) \times 10^{-6}$	$(4.3 \pm 0.4) \times 10^{-6}$
	$R_{L,t}$				$(1.9 \pm 0.2) \times 10^{-7}$	$(9.4 \pm 0.9) \times 10^{-7}$
$La_{0.4}Eu_{0.1}Ca_{0.25}U_{0.25}PO_4$	$R_{L,0}$	1	---	$(3.1 \pm 0.3) \times 10^{-4}$	$(1.8 \pm 0.3) \times 10^{-4}$	$(4.5 \pm 0.5) \times 10^{-4}$
	$R_{L,t}$			$(1.8 \pm 0.2) \times 10^{-5}$	$(7.2 \pm 0.7) \times 10^{-5}$	$(2.5 \pm 0.3) \times 10^{-5}$

1097 L.D. : Limit of detection

Table 5. Partial order related to the proton concentration and associated apparent normalized dissolution constant determined for several monazite-cheralite solid solutions. The extrapolated value of $R_L(U)$ at pH = 7 (T = 70°C) is supplied for comparison purposes.

	n	k_T' **(g.m^{-2}.d^{-1})**	**R_L(U) at pH =7 (g.m^{-2}.d^{-1})**
$Ca_{0.5}Th_{0.3}U_{0.2}PO_4$	0.11 ± 0.01	$(1.7 \pm 0.1) \times 10^{-3}$	$(2.9 \pm 0.3) \times 10^{-4}$
$Ca_{0.5}Th_{0.2}U_{0.3}PO_4$	0.20 ± 0.02	$(7.4 \pm 0.8) \times 10^{-3}$	$(2.9 \pm 0.3) \times 10^{-4}$
$Ca_{0.5}Th_{0.1}U_{0.4}PO_4$	0.12 ± 0.01	$(3.3 \pm 0.4) \times 10^{-3}$	$(4.8 \pm 0.5) \times 10^{-4}$
$La_{0.5}Ca_{0.25}Th_{0.15}U_{0.10}PO_4$	0.18 ± 0.02	$(1.1 \pm 0.1) \times 10^{-3}$	$(6.0 \pm 0.4) \times 10^{-5}$

Table 6. Values of log ($K_{S,0}°$) reported for some actinides and lanthanides phosphates (from du Fou de Kerdaniel et al. 2007)

Compound	Log ($K_{S,0}°$)	T (K)	Reference
$Th_2(PO_4)_2(HPO_4).H_2O$	– 66.6 ± 1.1	298	Clavier et al. 2006
$Th_{2-x}Pu_x(PO_4)_2(HPO_4).H_2O$	– 63.2 ± 1.1	298	Robisson et al. 2002
$LaPO_4$. ½ H_2O (rhabdophane)	– 24.5 / – 27.4	298	Jonasson et al. 1985
$NdPO_4$. ½ H_2O (rhabdophane)	– 26.0	373	Poitrasson et al. 2004
$PrPO_4$. ½ H_2O (rhabdophane)	– 25.7	373	Jonasson et al. 1985
$ErPO_4.nH_2O$ (xenotime)	– 25.5	373	Jonasson et al. 1985
$AmPO_4.nH_2O$	– 24.8 / – 27.2 ± 0.5	298	Rai et al. 1992 Robisson et al. 2002
$CmPO_4.nH_2O$	– 29.2 ± 0.4	298	Robisson et al. 2002
$Ca_{0.1}Nd_{0.8}Th_{0.1}PO_4$. ½ H_2O	*Work in progress*		
$(UO_2)_3(PO_4)_2.5H_2O$	– 55.1 / – 53.3	298	Sandino and Bruno 1992 Thomas et al. 2001

1109

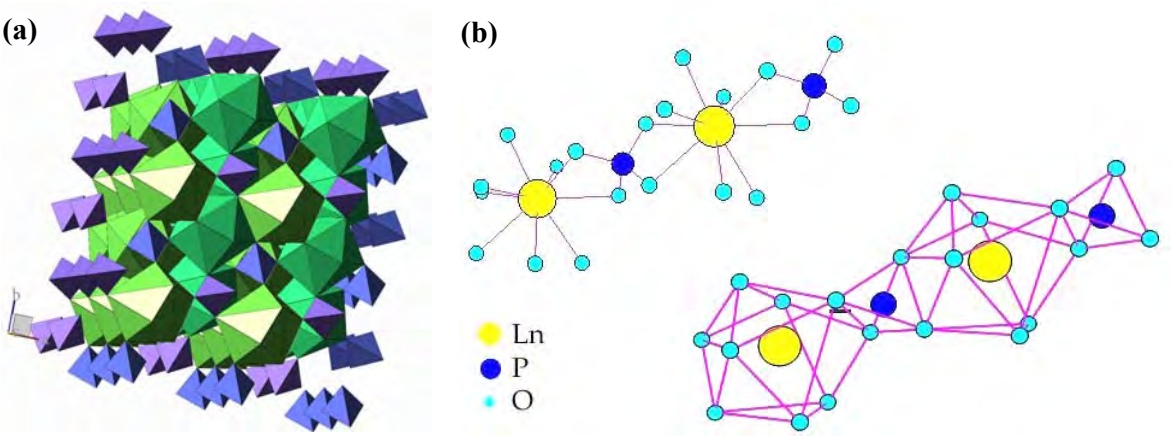

1110 **Figure 1.** Representation of the monazite structure (a) (from Ni et al. 1995) and LnO_9
1111 polyhedrons connection (b).
1112

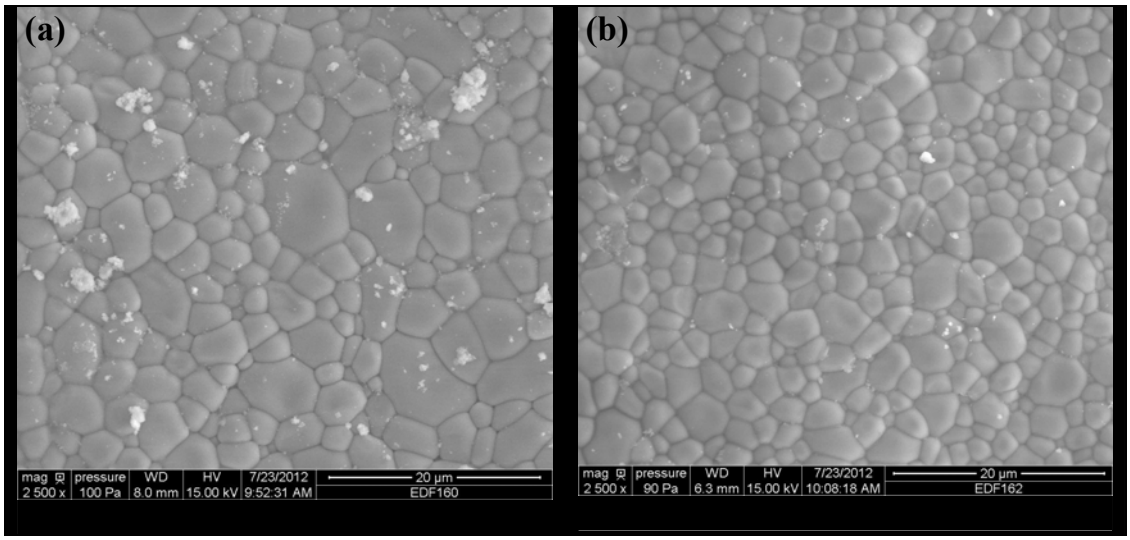

1113 **Figure 2.** SEM micrographs of $Ca_{0.5}Th_{0.4}U_{0.1}PO_4$ (a) and $Ca_{0.5}Th_{0.2}U_{0.3}PO_4$ (b) pellets
1114 sintered at 1300°C for 10 hours.

1115

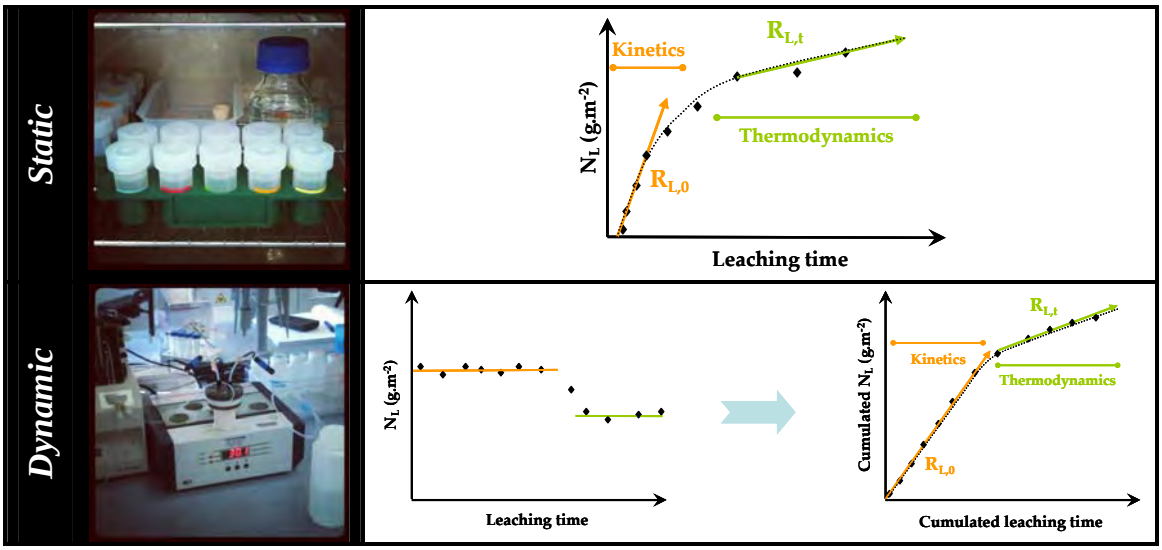

1116 **Figure 3.** Determination of $R_{L,0}$ and $R_{L,t}$ values during static and dynamic dissolution
1117 tests (inspired from Dacheux et al. 2010).
1118

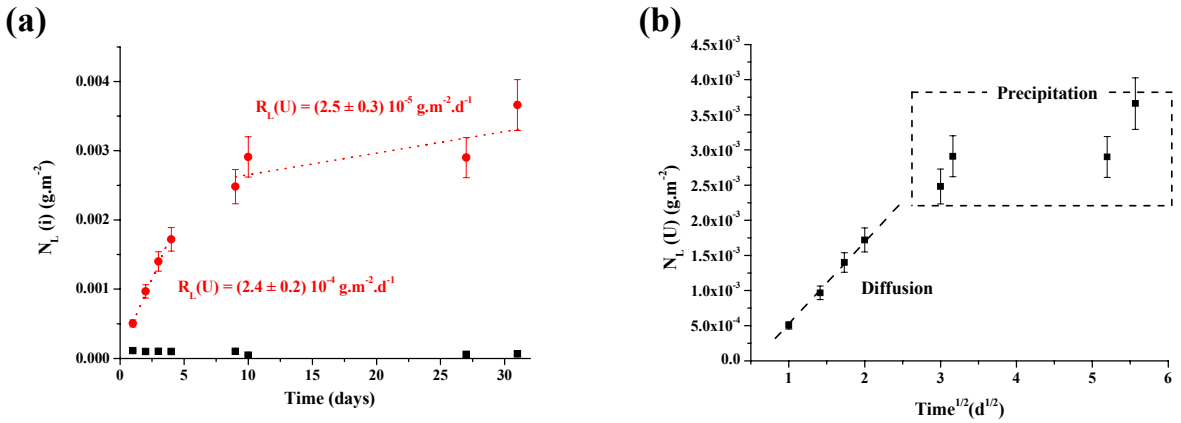

1119 **Figure 4.** Evolution of normalized mass loss during the dissolution of $Ca_{0.5}Th_{0.4}U_{0.1}PO_4$ (N_L(Th)
1120 (■), N_L(U) (●)) at T = 90°C (10^{-1}M HNO_3) (a) and variation of N_L(U) versus square root
1121 of time (b), revealing the apparition of diffusion phenomena (Lasaga 1998).
1122
1123
1124

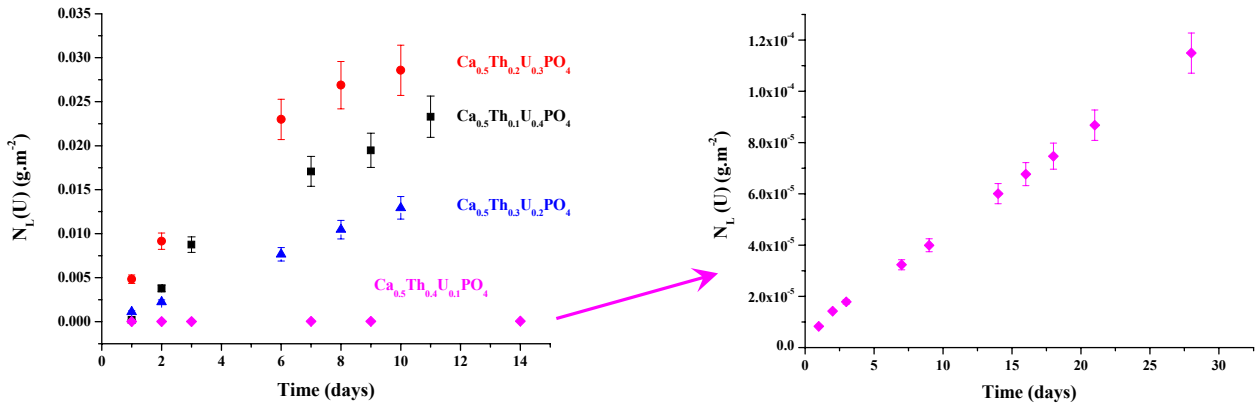

1125 **Figure 5.** Evolution of $N_L(U)$ normalized mass losses during the dissolution of $Ca_{0.5}Th_{0.3}U_{0.2}PO_4$,
1126 $Ca_{0.5}Th_{0.4}U_{0.1}PO_4$, $Ca_{0.5}Th_{0.2}U_{0.3}PO_4$ samples and of $Ca_{0.5}Th_{0.1}U_{0.4}PO_4$ in 10^{-1}M HNO_3
1127 (T = 70°C)
1128

1129

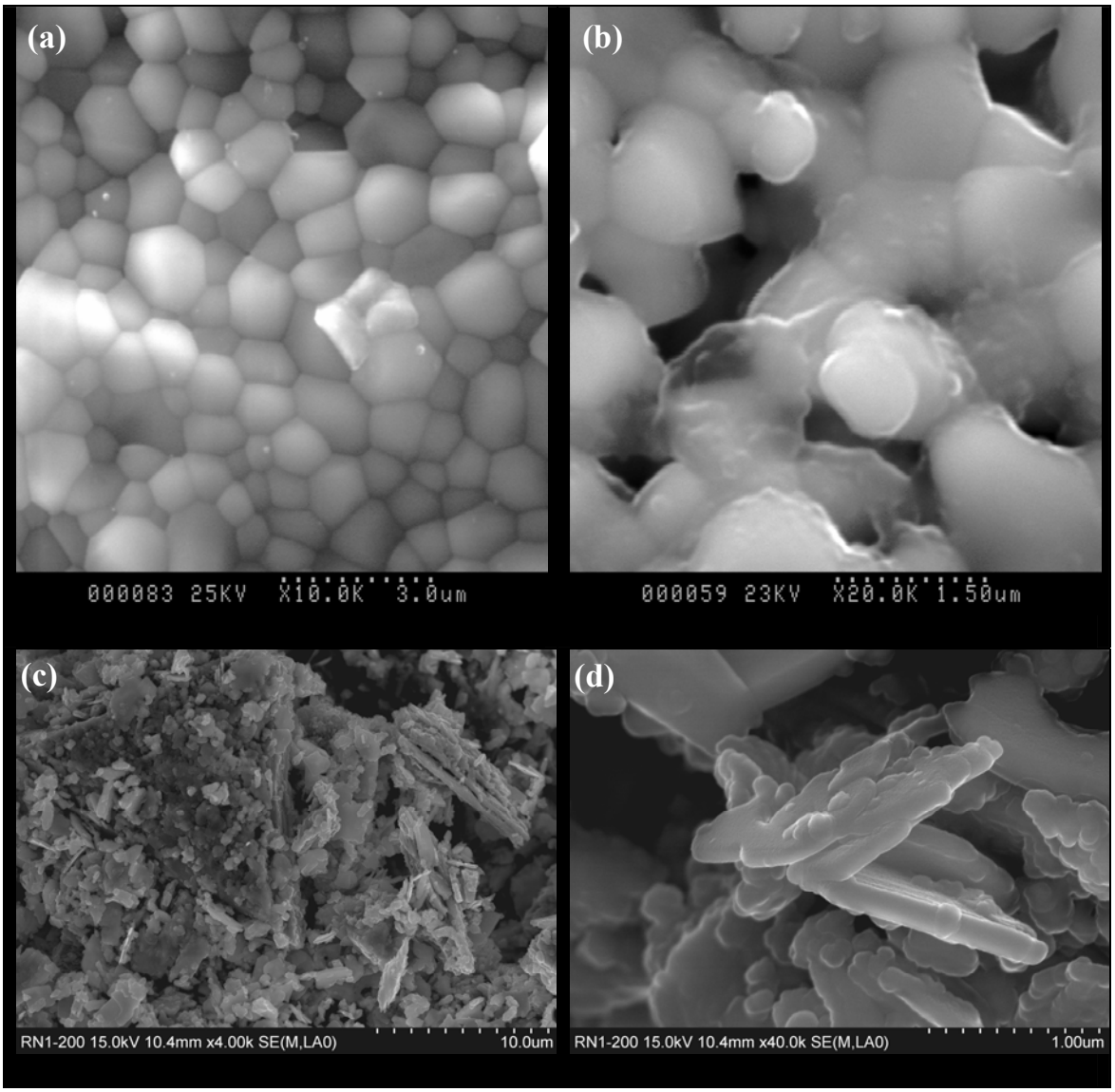

1130 **Figure 6.** SEM micrographs of leached $Ca_{0.5}Th_{0.5}PO_4$ pellets (a : 10^{-1}M HNO_3 and T = 90°C; b :
1131 10^{-1}M HCl and T = 70°C) and powder (c,d : 10^{-1}M HNO_3 and T = 90°C, t = 3 years)

1132

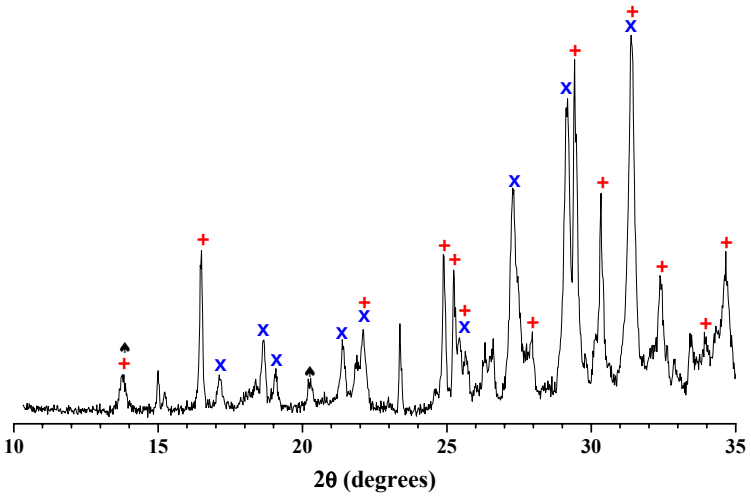

Figure 7. XRD pattern of $Ca_{0.5}Th_{0.5}PO_4$ powdered sample altered during 3 years in 10^{-1}M HNO_3 (T = 90°C). XRD lines of initial cheralite (x), TPHPH (+) and $Th(OH)PO_4$ (♠).

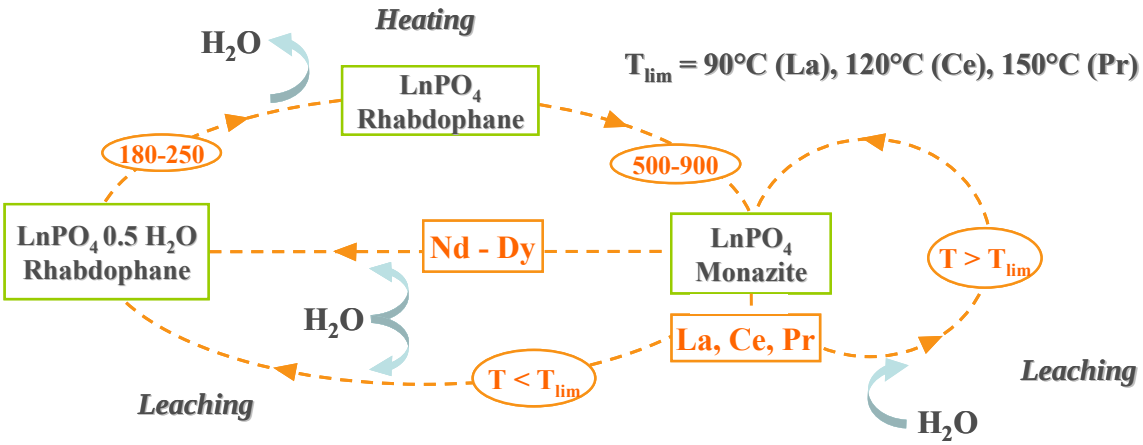

Figure 8. Links between rhabdophane and monazite during heat treatment or leaching steps of trivalent lanthanide bearing samples (after Clavier et al. 2007).